Lanthanides-based Upconverting Biolabels in the Near-Infrared

by

Marie-Pascale Manseau
B. Sc. McGill Univeristy, 2006

A Thesis Submitted in Partial Fulfillment
of the Requirements for the Degree of

MASTER OF SCIENCES

in the Department of Chemistry

Supervisory Committee

Lanthanides-based Upconverting Biolabels in the Near-Infrared

by

Marie-Pascale Manseau
B. Sc. McGill Univeristy, 2006

Supervisory Committee

Dr. ir. Frank C. J. M. van Veggel
Supervisor

Dr. Cornelia Bohne
Departmental Member

Dr. Robert G. Hicks
Departmental Member

Abstract

Supervisory Committee
Dr. ir. Frank C. J. M. van Veggel
Supervisor
Dr. Cornelia Bohne
Departmental Member
Dr. Robert G. Hicks
Departmental Member

Nanotechnology is more and more present in our world today and different fields are taking advantage of its possibilities. Among others, microscopists have been interested in using nanoparticles in combination with available techniques, one of which is fluorescence microscopy. Lanthanide-doped nanoparticles for example have been studied for many years now for their interesting luminescence and upconversion characteristics. This research presents the development of upconverting biolabels operating in the near-infrared (NIR) to eventually allow scientists to probe deeper into tissues using fluorescence microscopy. Two distinct types of nanoparticles were fabricated using the lanthanide ions Yb^{3+} and Tm^{3+} for their upconversion capabilities (from 980 to 800 nm) within the biological window (700 to 1000 nm). The first one, an annealed silica-coated LaF_3:Yb,Tm nanoparticle, could not be used as a biolabel due to its lack of dispersibility in aqueous environment. However, the second type, a silica-coated $NaYF_4$:Yb,Tm nanoparticles proved to be very promising. Two surface modifications of these particles were successfully performed. The first introduced NH_2 groups while the second incorporated polyethyleneglycol (PEG). The latter was achieved using two distinct methods: one through a reaction with the amino groups and one through a second silica coating involving PEGsilanes. Stable dispersions of these PEGylated nanoparticles were obtained and imaging of ovarian cancer cells grown in

their presence showed that they interact with the cells although the nature of this interaction is still to be determined.

Table of Contents

List of Tables

List of Figures

Acknowledgements

I would like to thank all the people that made this project possible for the past three years, first of all, my supervisor, Professor Frank van Veggel, who guided me through the labyrinth of synthesis and results and then my really good friend Dr. Chris Boyer without whom I could not have made through this. I would also like to acknowledge all the help that present and past members of the van Veggel group gave me in the lab. All this of course would have been impossible without the moral support of my friends here at Uvic, especially Saman and Katie. A special thanks also to my precious collaborators, Quinn Matthews and Conor Shaw from Andrew Jirasek's group here at Uvic and Rob Sahota from the DRC. I would also like to thank Glenda Catalano, Robert Iuvale and Derek Harrison from stores for their friendship and patience all these years. Finally, thank you to the University of Victoria and the Pacific Century Scholarship for their financial support.

Dédicace

Mes chers parents ; merci pour votre appui dans mes études mais surtout dans ma vie, je vous aime de tout mon coeur.

Lynne, Yves, Alexé et Jacob : vous êtes devenus ma deuxième famille et de toutes les belles choses que ma maîtrise m'a apportées, enfin apprendre à vous connaître est celle que je chéris le plus.

Éric Lavoie, Ghislain Bouchard et *Fredéric Dubé* : sans vous je n'aurais sans doute jamais autant aimé les sciences. Merci aussi pour votre amitié.

Marilyn Nadeau : merci pour ton inspiration dans mes études et dans ma vie. Tu m'as donnée la piqûre pour la chimie, et je te suis éternellement reconnaissante de m'avoir poussée à étudier en anglais.

Thank you to *all* my new friends here in Victoria, especially *Kate, Shannon* and *Charlotte*; without you life in Victoria would not have been half as good.

Chapter 1: Upconverting biolabels

1.1. Fluorescence

Fluorescence is an amazing optical phenomenon that can be observed all around us. Nature itself has developed a wide range of molecules and proteins that glow under UV light. This was brought to the attention of a larger public by television shows, where forensic experts employ UV lamps to detect biological samples on crime scenes. Chemical companies have also specifically developed fluorescence dyes for security purposes. Paper currency is a great example where such dyes are used on a large scale but it can also be used to identify rightful customers with ink stamps; for example, in big amusement parks like Disneyland or in some night clubs. Fluorescent light bulbs are also becoming more and more popular for their higher efficiency over tungsten-based lights. There are even some thoughts of replacing all tungsten bulbs with fluorescent ones in some provinces[1] and countries[2] around the world. So this phenomenon is all around us, but it is also very useful to a broad range of scientific disciplines like physics, chemistry, geology, and biology. Physicists have been studying fluorescence for years, chemists use it for analytical purposes[3], or quick and easy detection (in TLC plates for example). It is also an important tool to identify precious stones in geology[4] or to observe specific organisms[3] in biological systems.

Fluorescence occurs when a molecule, an atom or an ion, absorbs the energy from incoming electromagnetic radiation and reemits some of lower energy. This generally involves an electronic transition from a ground state to an excited state, followed by internal relaxation, then an electronic transition back to, or close to, the ground electronic state, during which light is emitted. In this typical scenario, a photon of high energy

(short wavelength) triggers the production of a photon of lower energy (higher wavelength); in this text, this will be referred to as regular fluorescence. The Jablonski diagram[3] (Figure 1) is widely used to summarize the concepts behind fluorescence and its difference with phosphorescence. The definition of fluorescence specifies that the emitted light must come from an electronic transition between two energy levels with the same spin multiplicity, most commonly between two singlet states. However, phosphorescence involves a change in spin, most commonly between a triplet and a singlet state. Luminescence is used as a more general term that includes all types of transitions no matter whether or not there is a change in spin.

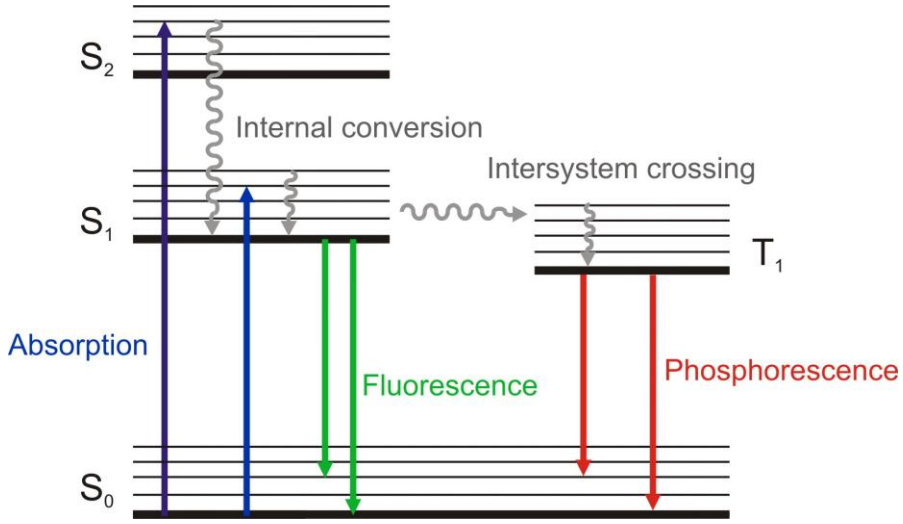

Figure 1: A simple form of the Jablonski diagram where S represents singlet states and T, triplet states.

Beyond that, there are some conditions under which two or more photons can combine their energy to trigger the emission of a photon of shorter wavelength. The two phenomena of this nature presented in this thesis are multiphoton absorption and upconversion. As in most of the literature, they are defined in this thesis as follow. Multiphoton absorption indicates that two (or more) photons are being absorbed basically

simultaneously by the fluorophore through intermediate virtual energy levels, followed by emission of a photon of shorter wavelength. Upconversion designates the emission of a photon of shorter wavelength after a *sequence* of absorptions or energy transfers; more on this below.

1.2. Multiphoton absorption

As for any absorption, multiphoton absorption is govern by the difference in energy of the energy levels of a molecules as well as by a series of selection rules[3], which, it is important to mention, differ from the selection rules for the absorption of a single photon. Multiphoton absorption implies the simultaneous (not sequential) absorption of two (or more) photons through the involvement of virtual energy states (dotted lines, Figure 2). Statistically, it is a rare event, facilitated at high excitation power densities (around MW/cm^2) because it requires two photons to meet both in time and space. As in the case of fluorescence, once the fluorophore is in an excited state, it can fluoresce which typically will be of shorter wavelength than the incoming photons. Multiphoton absorption is a non-linear process because a two-photon phenomenon depends on the excitation power density squared[5], a three-photon phenomenon depends on the excitation power density cubed[6], etc.

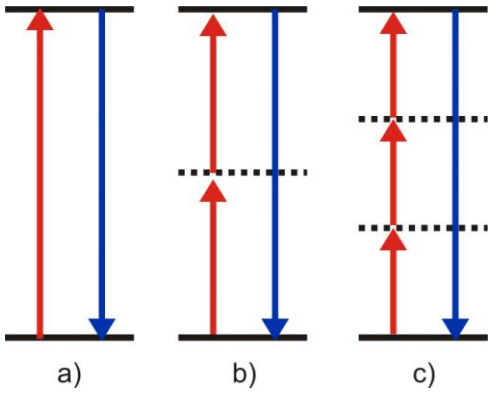

Figure 2: Comparison between one-photon, two-photon, and three-photon absorption leading to luminescence. a) Regular fluorescence; absorption of one photon leads to emission of one photon of equal or longer λ. b) Simultaneous absorption of two photons that leads to emission of one photon of shorter λ. c) Simultaneous absorption of three photons that leads to emission of one photon of shorter λ. The dotted lines represent a virtual energy level.

Multiphoton fluorescence is far less common in our lives than regular fluorescence; it is mainly put to advantage by scientists for spectroscopy[3] and microscopy[7] studies.

1.3. Upconversion in lanthanides

Luminescence, even more so upconversion, is different within lanthanide systems from what has been discussed above. Our group primarily focuses on some of the trivalent lanthanides ions where the luminescence observed comes from electronic transitions within the 4f orbitals which are shielded by the valence electrons in the 5s and the 5p orbitals[8]. These transitions are symmetry forbidden a partial mixing of the 4f orbitals with the 5d orbitals can allow luminescence of lanthanide ions. From the nature of the energy levels emerges one of the most important characteristics of the lanthanide ions: their photochemical robustness[9-11]. The transitions do not involve bonding orbitals as in the case of organic molecules but they occur inside the orbitals of the ions themselves; in organic molecules, the bonding (and the anti-bonding and the non-bonding) orbitals are

involved. In organic dyes, photobleaching[3] normally occurs when bonds are broken by rapid or intense vibrations or by the promotion of electrons from the bonding into the anti-bonding orbitals which weaken the molecule. In the lanthanides case, the energy is transferred to the surrounding (solvent, ligands, matrix, etc.) when undergoing internal relaxation processes and the crystal either dissipates the energy through lattice vibrations or the energy is absorbed by molecules surrounding it. As mentioned below, lanthanides ions are used widely for a range of applications taking advantage of their fluorescence characteristics. The relative position of the energy levels is essential to understand their behaviour (Figure 3).

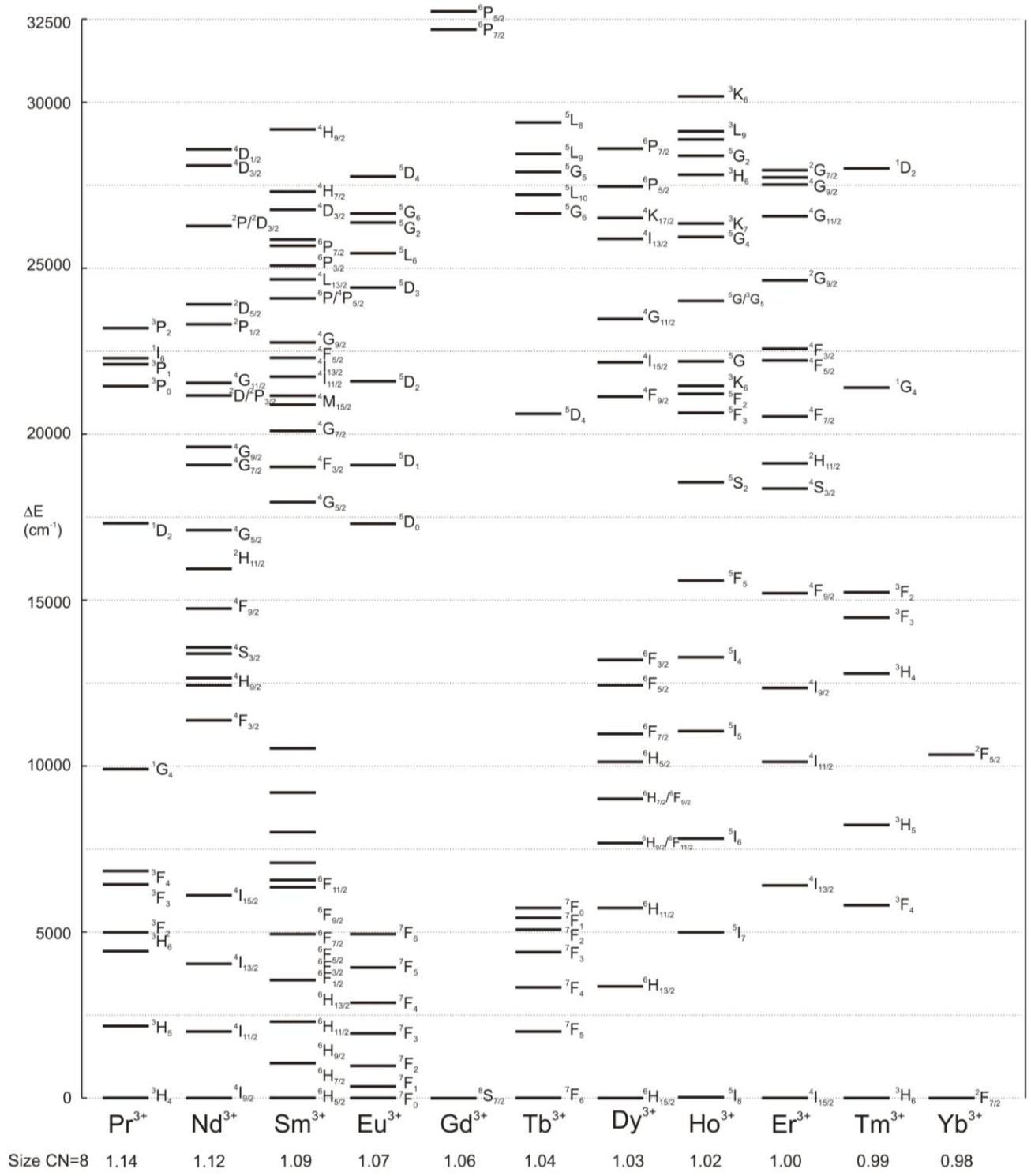

Figure 3: Energy levels[12] and sizes[13] of the trivalent lanthanides of most interest for Luminescence purposes (CN : coordination number).

The three elements of the lanthanide series not mentioned in Figure 3 are La^{3+}, Lu^{3+} and Ce^{3+}. The first two have a respectively empty, and full set of 4f orbitals, which means that there are no intra-4f electronic transitions possible in the UV-vis-NIR range. Cerium (III) is a special case; it has only one valence electron and one excited state, close to the ground state (at around 2500 cm^{-1}), which limits its use. On the other hand an allowed 4f-5d transition[8, 11] can be triggered by UV because Ce^{3+} has the lowest oxidation energy[8, 13] (easier to promote that electron out of the 4f shell) of all the lanthanides trivalent ions series.

The energy levels for the lanthanide ions series shown in Figure 3 are very well defined and are not greatly affected by the crystal field[8, 14]. The crystal field around the ions will splits each energy levels in sub-levels called Stark levels[8], which are within only hundreds of wavenumbers of each other[8], so the absorption and emissions for these ions are sharp[8, 14] and their position does not change significantly, although intensities might. This is very different from organic fluorophores where the luminescence comes from the bonding (and anti-bonding and non-bonding) energy levels which are subject to lots vibrations, giving rise to broad absorption and emission bands. This also makes the fluorescence of organics vulnerable to environment conditions like the pH or the type of solvent used.

The absorption and emission patterns of lanthanides are mainly influenced by the selection rules and then by quenching mechanisms which affect the lifetime of the excited states and alter the intensity of certain electronic transitions. This does not modify where the transitions occur on the energy scale but it can drastically influence which ones will be prominent. An important number of systems taking advantage of the

lanthanide ions luminescence incorporate the ions in a supporting matrix. A wide range of crystals are used, like $BaMgAl_{10}O_{17}$, widely used in fluorescent lamps[15] , Y_2O_2S and Y_2Si_2O, used in cathode ray tubes[15], and doped Nd:$Y_3Al_5O_{12}$ (Nd:YAG) crystals, used in lasers[16, 17]. These are only a few examples among a multitude but each of these has a specific phonon energy and specific crystal structure, where, in simple terms, a phonon is a quantum of a vibrational transition. Both greatly influence the internal non-radiative processes which, among others, affect the energy levels lifetimes. It is important to mention that the lifetimes of the levels responsible for the luminescence in lanthanide ions can be of the order[8, 14, 16] of μs or ms, well above typical lifetimes in organic molecules[3] (of the order of nanoseconds). This is an important advantage for some specific applications, solid-state lasers for example.

Lanthanides ions are known to enable upconversion processes with different mechanisms[5, 8, 16, 18]. "Energy levels assisted" is used here to emphasize that the system does not rely on virtual energy levels as in multiphoton processes (see Figure 2). The lifetimes of the levels involved will then have an important role to play in the efficiency of certain upconversion mechanisms versus others[19]. Upconversion in lanthanides involving only one ion normally goes through what is called ground-state absorption/ excited state absorption[8] as presented in Figure 4. It is a simple process where two photons are successively absorbed by a lanthanide ion. This phenomenon is facilitated by the long lifetimes of the energy levels in Ln^{3+} ions and allows such process to occur at power densities as low as a few watts per centimeters square (for the particles presented below, it has been observed at power densities around 15 W/cm^2).

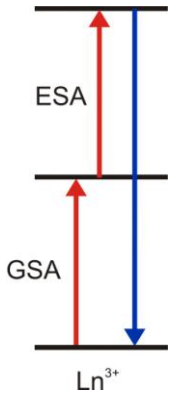

Figure 4: Schematic representation of the ground-state absorption (GSA) /excited state absorption[8] (ESA): an energy level assisted upconversion mechanism in lanthanides.

It is also very common to use more than one lanthanide ions to create a system where upconversion is enhanced by the interactions of such ions. A wide range of mechanisms[8, 18] has already been demonstrated in the literature and more are to be discovered but three basic ones are presented here. The first upconversion mechanism presented (as seen in Figure 5a) is the radiative energy transfer. In this case, a donor ion absorbs the energy of the incoming excitation and reemits a photon as if it was by itself. A nearby ion, the acceptor, then absorbs that photon and reaches an excited energy level. Before it has time to relax down to its ground state, another donor ion absorbs, and emits another photon, which can be absorbed by the acceptor ion to reach an even higher excited state. From there, it returns to its ground state emitting a photon of shorter wavelength than the excitation radiation. It is referred to as radiative energy transfer because the donor ion emits light. In opposition, a non-radiative energy transfer is observed when, as in Figure 5b, a donor absorbs the incoming radiation and transfers its energy to the acceptor without emitting light. This generally occurs mainly through dipole-dipole interactions. The acceptor ion is now in an excited state, and once again, before it has time to relax down to the ground state, another donor ion absorbs and transfers its energy to the

acceptor ion. The latter is now in a higher excited state from which it can emit light of shorter wavelength than the excitation beam.

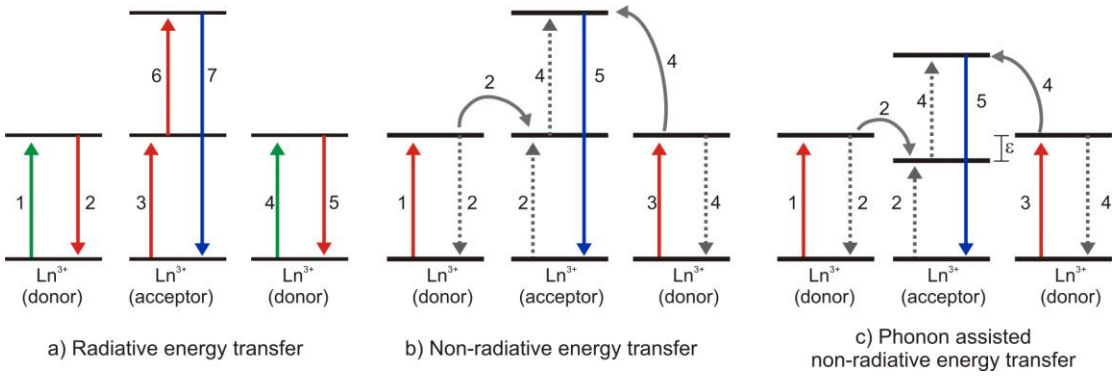

Figure 5: Three general categories of upconversion mechanisms for trivalent lanthanide systems[8]. The dotted lines represent non-radiative processes.

Finally, the last mechanism shown here (Figure 5c) is very similar to the previous mechanism because it involves a series of non-radiative energy transfers, the divergence in this case arises from the discrepancies in the energy of the levels involved. Energy transfers normally occur more efficiently in systems where the energy levels overlap, but inside a crystal structure, it is also possible to accommodate an energy gap (represented by ε in Figure 5c) by involving phonons. As previously mentioned, other mechanisms[8] like cooperative upconversion and photo-avalanche exist but are outside the scope of this thesis.

1.4. Upconversion in microscopy

Before exposing the benefits to take advantage of upconversion processes in microscopy it is important to explain some basic concepts. Transmission microscopy has been used by scientists for hundreds of years but incredible progress has been made since the Dutch Hans and Zacharias Janssen[20] put two lenses together to magnify small objects in 1590. The modern microscope is an assembly of lenses which collects light after it passes through the sample of interest. The contrast observed then arises from the difference in transmission properties of various parts of the sample. This was, and still is, extremely useful in numerous fields, especially biology, but sometimes it is of interest to distinguish two entities that have similar transmission characteristics. To solve that problem a multitude of dyes has been developed over the years to create artificial contrast between organisms. Another technique that has been used over time is fluorescence microscopy. Instead of looking at transmitted light, the fluorescence of the sample is observed. It is common that two systems having similar transmission characteristics will differ widely in terms of fluorescence characteristics. A generally better signal to noise ratio and lower detection limit[21] are other advantages of fluorescence microscopy. Soon, people developed dyes to be used in fluorescence microscopy to expand the range of possibilities. Watt W. Webb and Winfied Denk[22] then invented multiphoton microscopy in 1991 ; this new technique takes advantage of the statistics around multiphoton processes and longer excitation wavelength.

As mentioned earlier (section 1.2) multiphoton absorption requires a high power density which means that by tuning the intensity of the excitation laser properly, people are able to trigger multiphoton processes only at the focal point of the incident beam. Resolution

is then increased because only the focal point region will be excited and therefore fluoresces, which eliminates the need for a pin-hole as compared to confocal microscopy[23] and therefore increases the amount of light reaching the detector without compromising resolution. Another advantage comes from the fact that very few organic molecules will absorb the long wavelength used (typically in the NIR) in multiphoton microscopy. A lower absorption of the excitation wavelength by the surroundings reduces photobleaching, photodamage, and background fluorescence. Photodamage often leads to cell deaths, or simply to the destruction of the integrity of the specimen (denaturation of proteins for example), which means that multiphoton microscopy offers advantages for in-vitro and in-vivo measurements by lengthening the possible observation time. The major drawback with typical multiphoton microscopy is the imposing cost of the lasers needed to obtain high enough power density pulses.

As stated above, dyes have been developed over time to study samples with fluorescence microscopy. A lot of organic dyes[3, 24] and proteins[3] have been used, but quantum dots[25-29] and nanoparticles[14, 30-33] are becoming more and more popular for fluorescence microscopy. We are interested in lanthanide based inorganic particles and our group[34], among others[32, 35], have shown their potential as potential biolabels.

Table 1: List of pro's and con's for fluorescent organic dyes and luminescent inorganic nanoparticles.

Advantages	*Disadvantages*
Fluorescent Organic Dyes	
Well-known characteristics	Photobleach
Wide range available	Normally excited in the UV or Vis
Lots of different colours	Short lifetime (< ns)
Bioconjugation procedures well-established	A lot of them have small Stokes shifts
Luminescent Inorganic Nanoparticles	
Do not photobleach	
Large stokes shift	Stability in biological fluids can be an issue
Chemical stability	No extensive proof of non toxicity
Expected biocompatibility	Cell intake unknown
Long lifetimes (μs to ms)	Unknown impact on the environment

Logically, people now wish to develop fluorophores (dyes, or particles, or quantum dots) to be used in combination with multiphoton techniques. This is where the upconversion nanoparticles[36-40] come into play. We wish to create efficient upconverting particles that could be used for various biological studies and take full advantage of the biological window.

1.5. Biological window

The biological window is a term used by microscopy experts to designate a region of the electromagnetic spectrum, between 700 to 1000 nm, where biological samples are most transparent[21]. Therefore it is of great interest[21] to develop labels that would operate within that range to hopefully allow measurements to be performed deeper into tissues. The transparency of biological samples at these wavelengths can be explained by a balance between the optical characteristics of their two major components: water and organic molecules. The absorption spectrum of water is presented here in Figure 6.

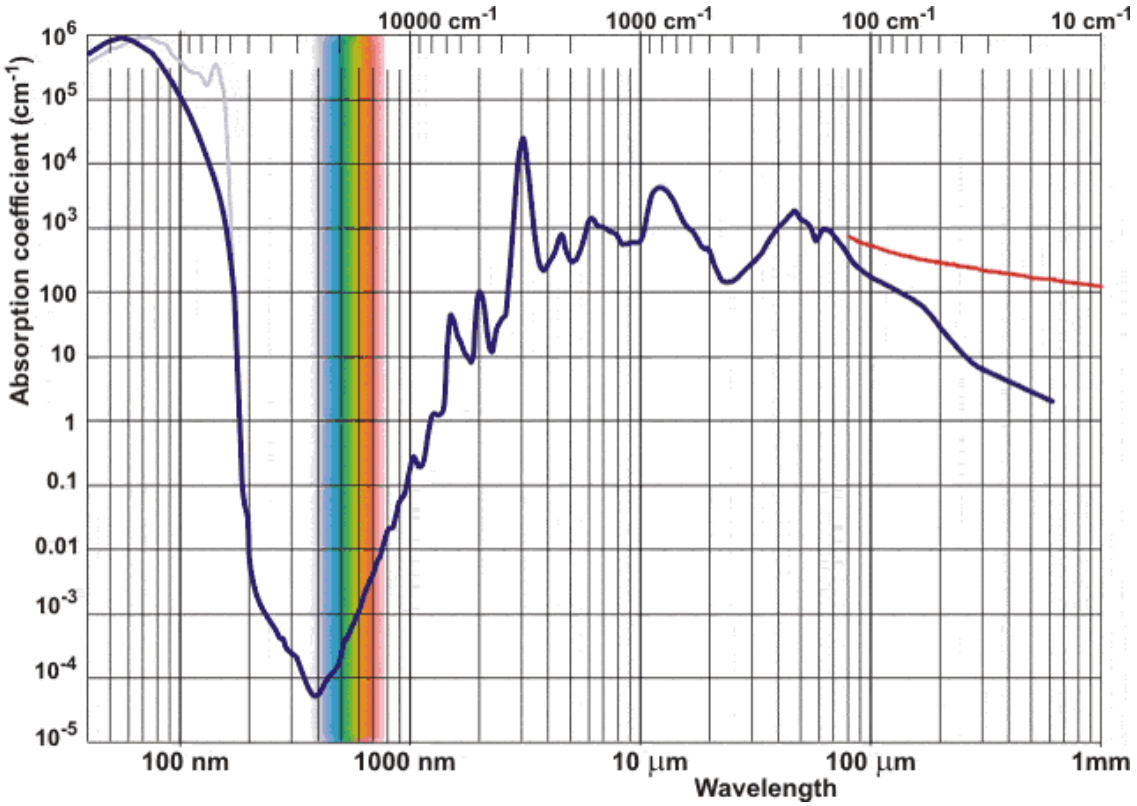

Figure 6: Absorption spectrum of water[41].

This spectrum shows that the absorption coefficient of water is below 0.1 cm^{-1} between 200 and 1000 nm with a minimum around 400 nm. Because living organisms are mainly composed of water, one could think that the biological window should be in the UV but this reasoning does not take into account the presence of organic molecules. Such species absorb in the UV and in the visible range therefore the biological window is considered to be in the NIR, where the combined absorption of organics and water is minimal. This explains another advantage of multiphoton absorption which by its nature generally uses excitation wavelengths within this region of the spectra. This allows excitation deeper in a sample and reduces the amount of background fluorescence. Additionally, shorter wavelengths are more efficiently scattered[42] which implies that UV

radiation scatters more than NIR radiation; this also contributes to a better penetration in biological samples. This is the most coveted aspect of our material.

1.6. Conclusions

In conclusion, fluorescence and other luminescence phenomenon have been used in microscopy to observe samples in various conditions. Fluorescence, multiphoton absorption, and energy level assisted upconversion are among the interesting optical processes that can be used microscopy. Their mechanistic differences are summarized by the following Figure.

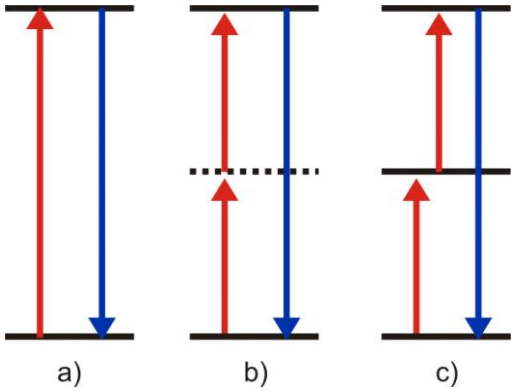

Figure 7: Comparison between a) fluorescence, b) two-photon absorption, c) energy levels assisted upconversion. The dotted line represents a virtual energy level.

Both the multiphoton absorption and the upconversion mechanism involve multiple photons of long wavelength to generate photons of shorter wavelength but the upconversion often requires lower power densities because it takes advantage of energy levels present in the system instead of virtual energy levels. The development of new fluorophores for each of these methods, no matter what they are, organic molecules, inorganic particles or quantum dots, opens the door to measurements of different systems under new conditions and widens possibilities for biologists. The development of a new

type of biolabel which excitation and emission would be within the biological window would be profitable to observe features deeper into live samples. This is the objective pursued in the next chapters of this thesis.

Chapter 2: First type of particles : LaF_3 nanoparticles

2.1. Introduction

2.1.1. Why use nanoparticles?

Lanthanides ions complexes in solution have been used for a long time as fluorescent biolabels for a wide range of studies[43, 44]. They are especially valuable tools for DNA assays[44] but in other cases having these ions encapsulated in a particle also proves to have advantages. First, it shields the ions from solvent molecules, reducing unwanted interactions responsible for energy quenching. A wide range of matrices to encapsulate lanthanide ions have been explored over the years for different purposes. Few examples or $Y_2O_2S:Eu^{3+}$ and $LaPO_4:Ce^{3+}$ used in light displays and $YAG:Nd^{3+}$ used in solid state lasers. As previously mentioned (section 1.3), the nature of the emission from lanthanide ions is not significantly influenced by its environment (solvent, pH etc.), but the lifetimes of the energy levels and the efficiency of the energy transfer processes are. When the Ln^{3+} ions are part of a crystalline structure, the symmetry of the crystal field and the phonon energy of the matrix will affect the observed emission by favouring, or not, certain transitions. The incorporation of ions in a particle also allows to group ions, of the same nature, or not, in a close environment. This is essential for some of the upconversion mechanisms[5] known for lanthanides trivalent ions. So grouping ions is important for energy transfer mechanisms but an optically neutral matrix is often necessary to dilute them: too many emitting ions close to one another give rise to self-quenching and self-absorption[8]. Self-quenching indicates the quenching of the emission of one ion by a neighbouring ions of the same nature, while self-absorption indicates the absorption of the light emitted by a neighbouring ion of the same nature. These

phenomena are known to change the fluorescence characteristics and efficiency of the material. This is the reason why most materials taking advantage of the luminescence capabilities of the trivalent lanthanide ions are matrices doped with a low percentage of emitting ions. Generally, emitting Ln^{3+} ions concentrations range from a few hundredth percent to 0.05-0.1% although donor ions (often Yb^{3+}) concentrations can be much higher (anywhere from 0 to 100%).

Lanthanides nanoparticles also offer advantages compared to other methods available for biolabelling like organic fluorophores[3] and quantum dots[29]. It is important to emphasise that the nature of luminescence in the lanthanide ions is different from the one seen in organic dyes or quantum dots[45]. Luminescence from organic dyes involves bonding, anti-bonding and non-bonding energy levels which are subject to a lot of vibrations while in quantum dots, the energy level structure in spanned by the quantum confinement of the exciton due to reduced size of semiconductors. One of the most important advantages of Ln^{3+} ions is certainly their robustness, especially their photostability. The trivalent lanthanide ions can go through an infinite number of photocycles without being affected: they do not photobleach. This is an important advantage over organic molecules that can sustain only a certain amount and frequency of incoming energy before breaking down and losing their fluorescence[3] characteristics. Quantum dots are better than organic fluorophores on that aspect, but they are still not as resistant as lanthanide ions. Only a change in the nature of the ions through something like a reduction would modify the energy levels along with the fluorescence characteristics of the ions, but this is not known to occur due to photoexcitation. Most lanthanide nanoparticles[34, 37, 46] present in the literature are not air or moisture sensitive (they do not degrade under these conditions)

which is also an issue with some quantum dots[47]. Another advantage of the lanthanides ions is the large energy gap between their excitation and emission bands. This eliminates technical problems arising from excitation and emission overlap, especially in microscopy where the excitation has to be filtered out of the emission signal. As discussed above, the emission wavelength of Ln^{3+} doped nanoparticles will not significantly vary with size, or other characteristics of the particles environment, like pH. This simplifies identification and facilitates multiplexing.

The first type of particles presented here is based on a lanthanum trifluoride matrix doped with two emitting lanthanide ions: Tm^{3+} and Yb^{3+}. La^{3+} has an empty 4f shell and therefore does not absorb visible light. The notation used for the composition of the nanoparticles is the following: LaF_3:Ln,Ln where the Ln represent any lanthanide trivalent ion as a dopant. Over the years, our group has developed a simple synthetic route at low temperature to produce doped LaF_3 nanoparticles stabilized with citrate ligands. The phonon energy and the crystal field of fluorecite was found suitable to allow emission of a wide range of the lanthanide ions and has been used for various projects within our group[48-51] and others[51-54]. Unfortunately these nanoparticles typically do not exhibit upconversion because of quenching from the ligands and solvent. One way to solve this problem is to build a shell around the particle materials like[55] ZrO_2, TiO_2 and Al_2O_3; we opted for a silica shell (SiO_2) for its biocompatibility. Silica coating is already found in various materials to render them biocompatible[30, 56]. Some quantum dots[28, 57-60] and nanoparticles[30, 61, 62] experts are already employing it widely. It is also a very well studied[63-65] surface that should simplify functionalization of the particles, allowing specific labelling. When incorporated in Tm^{3+} is very sensitive to quenching through

water and OH groups so for the first material presented here, it was essential to perform an annealing step to enable upconversion. The final nanoparticle discussed in this chapter is a baked silica-coated LaF_3:Yb_{20},Tm_5 nanoparticle; later on the subscripts are omitted for clarity.

2.1.2. Optical properties of Yb^{3+} and Tm^{3+} doped nanoparticles

The photophysical properties of this system come from the two trivalent lanthanide ions: Tm^{3+} and Yb^{3+}. The latter absorbs the incoming excitation radiation and transfers its energy to Tm^{3+} which emits in return. It is essential to use Yb^{3+} because of its larger absorption cross section ($9.2 \times 10^{-21} cm^2$)[66] and its facility to transfer its energy to nearby ions like Tm^{3+}. The important energy levels for this study are shown in the following Figure.

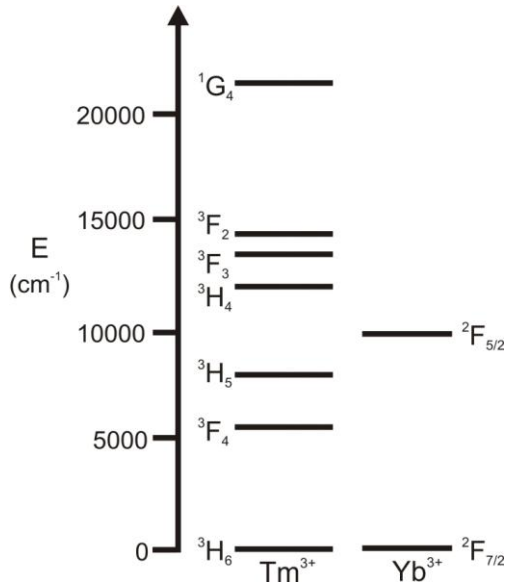

Figure 8: Energy levels[12] of the trivalent lanthanide ions of interest: Yb^{3+} and Tm^{3+}.

From this, one can see how simple the energy level structure of the Yb^{3+} ion is. Its only energy level above ground state corresponds approximately to the energy of a 980 nm photon. However, the level structure of Tm^{3+} is far more complex and gives rise to

interesting luminescence. The mechanism involved in the upconversion observed for this specific system is called a phonon-assisted non-radiative energy transfer[8]. As demonstrated later on, two prevailing emission lines can be observed when measuring the upconversion of the nanoparticles, one at 800 nm and one at 475 nm. The first one, in the near-infrared region, is a result of a two-photon process (Figure 9).

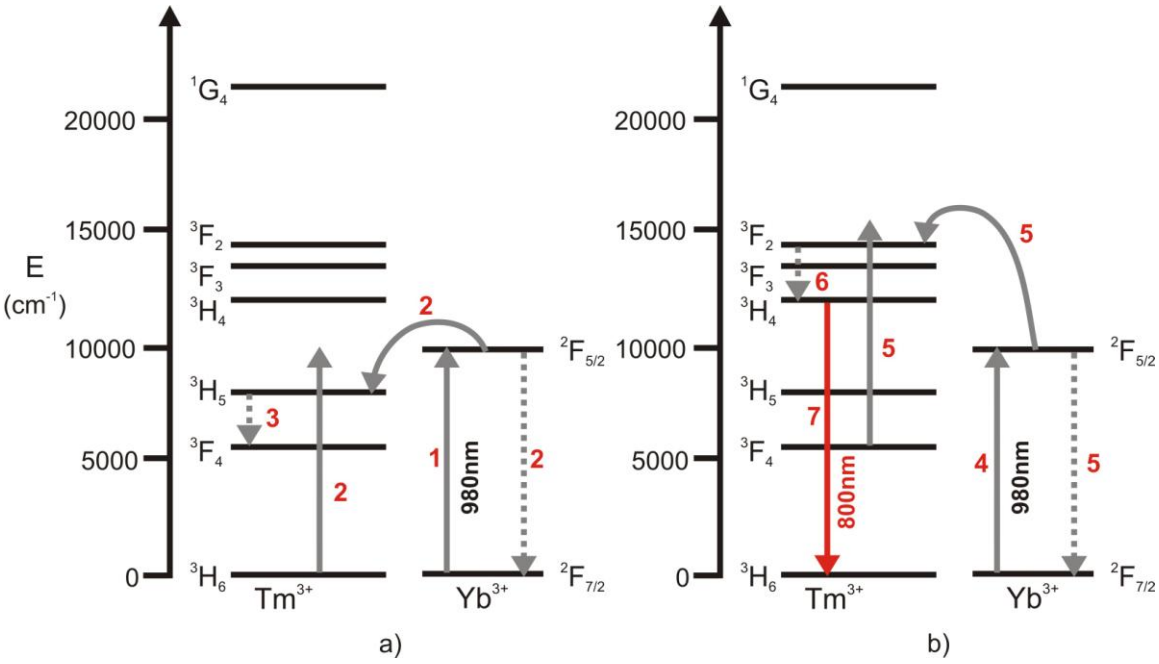

Figure 9: Upconversion mechanism[8] occurring in an Yb^{3+} - Tm^{3+} system to produce an emission at 800 nm. The numbers represent the sequence of events.

As illustrated by Figure 9, the Yb^{3+} ion absorbs the 980 nm excitation radiation, transfers its energy to the Tm^{3+} ion; a non-radiative process which necessitates the help of a few phonons because of the slight discrepancy in energy of the two levels involved (ca. 2050 cm^{-1}). The Tm^{3+} then relaxes down through a non-radiative process but the $^3F_4$ energy level of Tm^{3+} having a relatively long life time, it allows another nearby Yb^{3+} ion to absorbs another 980 nm photon and transfer its energy to the Tm^{3+}as well. The Tm^{3+} then reaches a higher excited state ($^3F_2$) than the energy associated with one photon from

the excitation source. After an internal relaxation to level $^3H_4$, Tm^{3+}, among other things, can emit a 800 nm photon. A very similar mechanism, involving three photons instead of two, is responsible for the production of 475 nm light as shown by Figure 10.

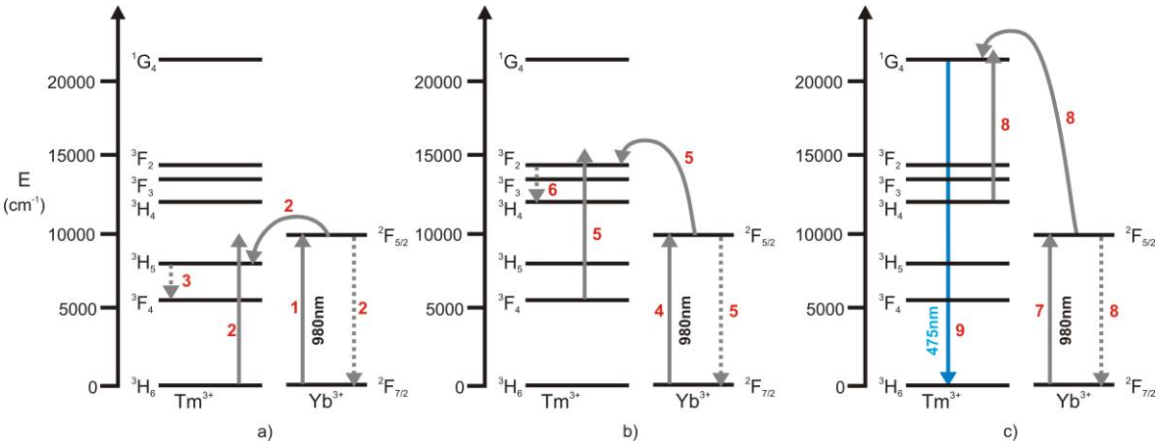

Figure 10: Upconversion mechanism[8] occurring in a Yb^{3+} - Tm^{3+} system to produce an emission at 475 nm. The numbers represent the sequence of events.

In this case the ions undergo the exact same sequence of events as explained earlier, except that before it has time to emit a photon at 800 nm another Yb^{3+} ion transfers more energy to Tm^{3+} and excites it to $^1G_4$ level from which it can emit a 475 nm photon.

This summarizes the important photophysical properties of baked silica-coated LaF_3:Yb,Tm nanoparticles. The following sections present the synthesis as well as the obtained results.

2.2. LaF_3 based nanoparticles synthesis

2.2.1. Experimental details

The following chemicals were used for the synthesis below. From Aldrich : lanthanum(III) nitrate hexahydrate 99.999% ; thulium(III) nitrate pentahydrate 99.9%; ytterbium(III) nitrate pentahydrate 99.9%; sodium fluoride 99% ACS reagent. Also, citric acid monohydrate powder reagent ACS from ACP; anhydrous ethyl alcohol from

Commercial Alcohols; tetraethoxysilane (TEOS) 99+% from Gelest and ammonium hydroxide with 28.0 to 30.0% NH_3 content from Caledon. All these products were all used as received without further purification.

The samples were centrifuged using a Beckman Coulter Spinchron 15 (rotor F0630). For annealing, the samples were placed in small quartz crucible and in a tube furnace from Landberg/Blue M (model #HTF55322A). The sonicator used is from Branson (model #3510) and the X-ray diffraction (XRD) patterns were produced using a powder X-ray diffractometer from Rigaku called the Miniflex which uses a 1.8kW Cr X-ray tube. The XRD patterns analysis was performed with the Materials Data Inc program JADE 8.2. The reference patterns for the XRD patterns were retrieved from the International Center Diffraction Database RDB inorganics 56/61189. The patterns presented here were smoothed using adjacent averaging of 5 points and the background was removed manually. The Transmission Electron Microscope (TEM) were measured with a Hitachi H-7000 Transmission Electron Microscope equipped with a tungsten filament (75 kV) and a AMT 2k x 2K CCD camera. Finally, the upconversion measurements were performed with a FLS 920 fluorescence system from Edinburgh instrument combined with a 980 nm continuous wave (CW) diode laser from JDS Uniphase (devise type 63-00342) coupled to a fibre optic with a core diameter of 105 μm. It was powered at 1.05 A (~ 20 W/cm^2) by a 2400-C SourceMeter power supply from Keithley however, for the picture, a programmable power supply PSP-2010 from GW Instek was used to power the diode instead (at 5 A ~ 150 W/cm^2). The measurements were done on KBr pellets; the slits were opened for 1 nm resolution; a 850 nm low pass filter (wavelengths shorter than 850 nm blocked) was put in front of the laser and a 800 nm high pass filter (wavelengths

longer than 800 nm blocked) before the monochromator. The spectra are an accumulation of 5 scans (10 for the measurements of the blue emission) and the dwell time used was 0.2 s. The spectrum of the 800 nm emission is cut at 825 nm because of the use of the 800 nm high pass filter.

2.2.2. Core LaF_3:Yb,Tm Synthesis

The synthesis previously developed by our group[67] to prepare doped nanoparticles of LaF_3 is amazingly simple. A total of 1 mmol of lanthanide nitrate salts, divided into the desired molar fractions, is dissolved into 2 mL of methanol. For example, in this case, 0.75 mmol of $La(NO_3)_3 \cdot 6H_2O$, 0.20 mmol of $Yb(NO_3)_3 \cdot 5H_2O$ and 0.05 mmol of $Tm(NO_3)_3 \cdot 5H_2O$ were used. Likewise, 3 mmol of NaF is dissolved into 2 mL of distilled water. These are then added dropwise, sequentially, to a solution at 75 ºC of 2 g of citric acid in water, with its pH adjusted to 6 with NH_4OH. The solution should be clear and colourless and allowed to react for 2 hours after which it is cooled to room temperature. After precipitation of the particles through a slow addition of 60 mL of absolute ethanol, they were centrifuged at 5000 rpm (2180 × g) and washed three times, still with absolute ethanol, and dried under reduced pressure. The final product is about 200 mg of a fine white powder. It disperses readily in water; it can be stored for a long period of time without noticeable degradation, although extensive drying the sample might result in the formation of aggregates and a loss of dispersibility.

2.2.3. Silica coating of the nanoparticles

A wide range of variables of Stöber[68] process influenced synthesis were used over the progress of this project but here is a description of the conditions that gave us the best results.

About 10 mg of the LaF_3:Yb,Tm nanoparticles are dispersed into 5 mL of water, vortexed and sonicated to reach a good dispersion. These were then added dropwise to 40 mL of absolute ethanol in a round bottom flask suspended in a sonicator. Adding gradually enough ethanol leads to a clear dispersion. A 1:1 solution of TEOS in ethanol was also prepared (the quantities of TEOS used normally ranged from 0.1 mL to 1.2 mL) and added dropwise to the flask.

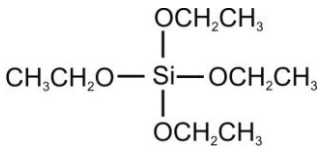

Figure 11: Chemical formula of tetraethoxysilane (TEOS)

Finally 0.5 mL of NH_4OH was added very slowly and let to react. The most typical reaction time used was around 1 hour because in most cases the reaction mixture would turn slightly hazy by that time. The isolation of the particles has always been a challenge and various techniques were explored over the time but in the end it seemed that centrifuging at high speed , 12000 rpm, ($12557 \times g$) was the best way to do so. Reducing the amount of solvent by evaporation has also been used, in combination with centrifugation on occasion. The drying procedure was also varied but it seems like drying under vacuum for about 30 min (depending on how wet the sample coming out of the centrifuge was) leads to a suitable product.

At this point the sample does not show any upconversion because of extensive quenching from water and OH groups. It is essential to annealing these samples to achieve upconversion.

2.2.4. Annealing

Three different baking schemes were used to eliminate quenching from the OH groups in the LaF_3:Yb,Tm silica-coated nanoparticles and allow upconversion. They are presented in Table 2 below.

Table 2: Baking schemes used for annealing of silica-coated nanoparticles.

Baking schemes:	Starting Temperature ºC	Final Temperature ºC	Ramp time up h	Ramp time down h	Plateau time h	Total time h
Baking scheme #1	25	800	4	4	24	32
Baking scheme #2	25	800	1	1	24	26
Baking scheme #3	25	800	24	24	24	72

2.3. Results and discussion

LaF_3 nanoparticles doped with about 20% of Yb^{3+} and 5% of Tm^{3+} were synthesized easily in water with citrate ligands. These were subsequently silica coated using a Stöber process and annealed at high temperature (800 ºC) to remove all traces of water and OH groups that quench the desired upconversion.

The annealing process is very complicated and might be optimized to favour different emissions but this could be a thesis in itself because annealing processes are very complex and tricky to unravel. So although three different baking schemes were briefly explored, in the end, it was decided to stick with the first one (see Table 2) because no obvious differences were noted when comparing the properties of the obtained samples.

In all cases, a change in appearance occurred during the annealing although the samples remained white. Some would appear very glassy, almost translucent (Figure 12), and others would be more powdery. The samples were stored in small glass vials and remain stable over long periods of time.

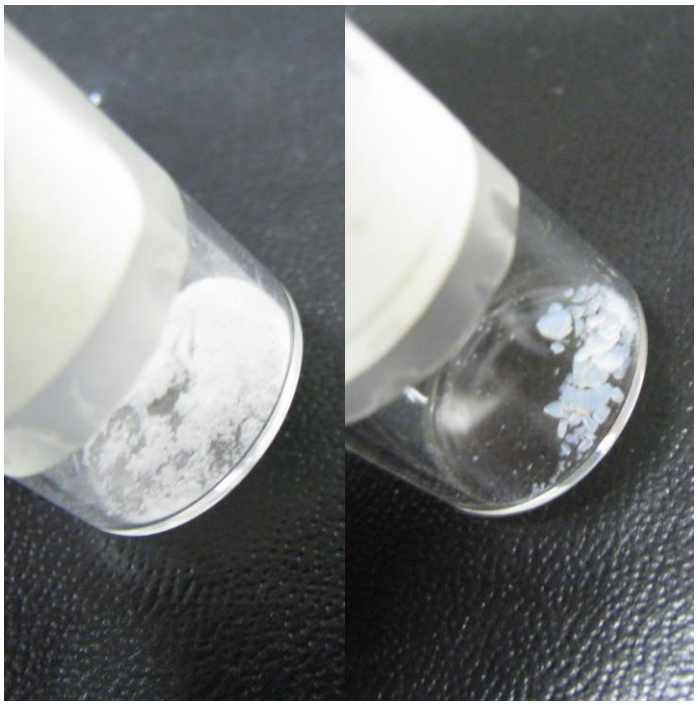

Figure 12: Example of appearance change observed after annealing. A silica-coated sample: before (left hand side) and after (right hand side) heat treatment.

In order to observe the silica-coated particles, the most precious tool was undeniably TEM (transmission electron microscope). Unfortunately, with the TEM at the University of Victoria, the contrast was not good enough to observe the individual core particles (LaF_3:Yb,Tm) before silica coating. This is consistent with a size of 4-5 nm in diameter as determined in the past[34] by previous group members but an analysis of XRD patterns was also used to corroborate this.

2.3.1. X-ray Diffraction of the doped LaF_3 core

A powder X-Ray diffraction (XRD) analysis of the LaF_3 nanoparticles first allowed the confirmation of the nature of the nanoparticles by identifying the fluorecite crystal phase (Figure 13).

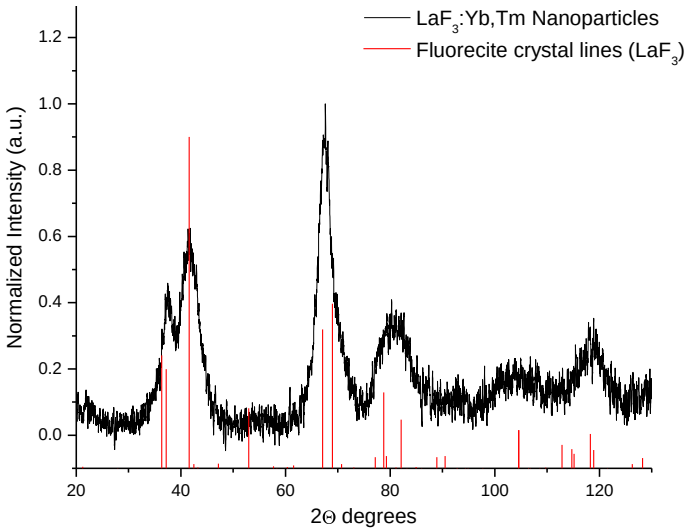

Figure 13: XRD pattern of some core nanoparticles, LaF_3:Yb,Tm identifying the fluorecite crystal phase (PDF#01-072-1435).

As can be seen in this figure, the XRD peaks are broadened because of the small size of the crystal so it was possible to estimate particle size present in the samples. As mentioned in the experimental details, this was done using an automatic function called peak fitting included in the XRD treatment software JADE. This tool uses the Scherrer's equation[69] to relate the broadening of XRD peaks with the crystallite sizes. From this analysis, the sizes were determined to range between 3 and 6 nm. It is important to mention this is not meant as an absolute way to measure sizes but only to corroborate other observations. It is not very precise for such small particles but it certainly allows us to confirm the sizes to be below 10 nm as supported by TEM results as well as past experiments done within our group. The next step was to look into the silica coating of these small nanoparticles.

2.3.2. TEM

TEM was an important tool to observe the final particles because the electron density varied greatly between the core and the shell. Multiple samples were observed and a

large range of results was obtained. Silica coating is a straightforward procedure but to obtain individual, well-defined particles is a challenge. Imperceptible changes in experiment conditions seemed sometimes to have a large effect on the final outcome. It was possible to look at the reaction mixture itself by dipping a TEM grid in it because the concentrations were not high enough to significantly impair the measurements.

Early on, various problems arose during the silica coating procedure. One common problem was the formation of silica beads (without a luminescent core) along with the desired silica-coated LaF_3 nanoparticles (Figure 14).

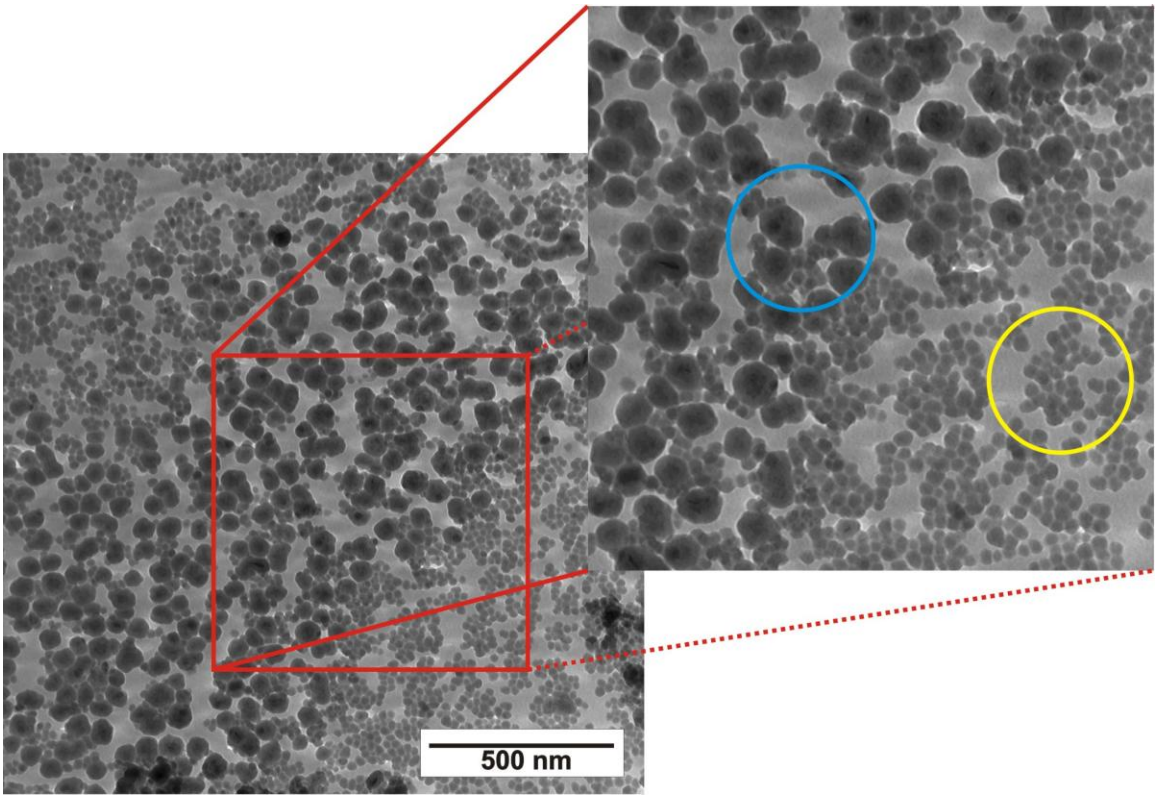

Figure 14: TEM of a sample demonstrating the problematic formation of silica beads. The blue circle represents silica-coated LaF_3:Yb,Tm particles and the yellow circle shows the silica beads.

Excessive aggregation or ill-defined particles was also an important problem encountered as shown in Figure 15. Instead of the silica forming individual particles, sometimes the

formation of larger networks also occurred. This could have been caused by higher concentrations of core particles initially used.

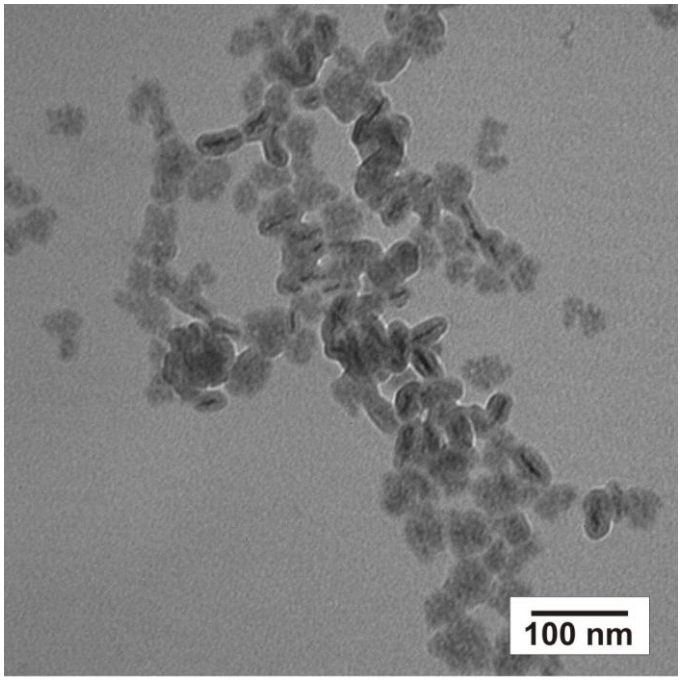

Figure 15: Example of aggregated and ill-defined silica-coated LaF_3.

Eventually, by changing slightly the reaction towards the conditions described earlier, an acceptable product was reached. The reaction mixture of such successful attempt looked like Figure 16. In this case, the particles are well-defined, no network is apparent, all the particles contained a LaF_3 core and even the biggest aggregates present were shorter than 200 nm.

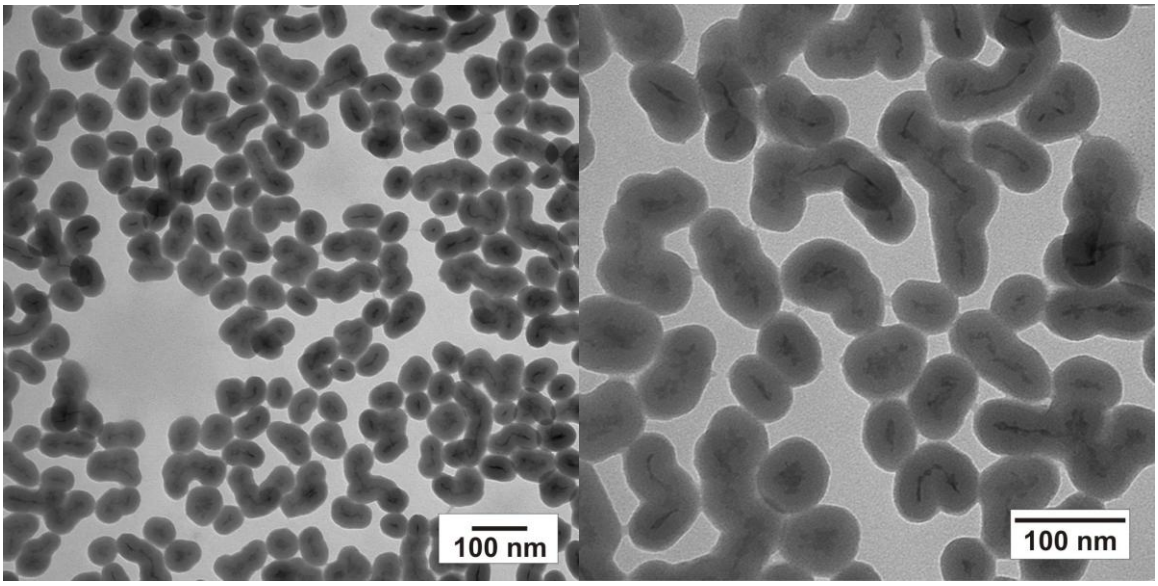

Figure 16: TEM of a reaction mixture showing nice silica-coated particles.

The remaining aggregation problem comes from the fact that the core particles seem to form bigger, non- spherical cores in the centre of the silica shell. This is not a problem in itself but it reduces the uniformity of the samples and some of the particles end up much longer than others. Perfect monodispersity and uniformity is not an immediate requirement but it would certainly be advantageous for some applications, especially quantitative applications like assays.

The isolation process itself is also problematic because theoretically a perfectly dispersible particle will not want to come out of solution so some of the best particles can be lost at this stage. It was however possible to obtain an acceptable final product (Figure 17) where most of the particles are below 100 nm.

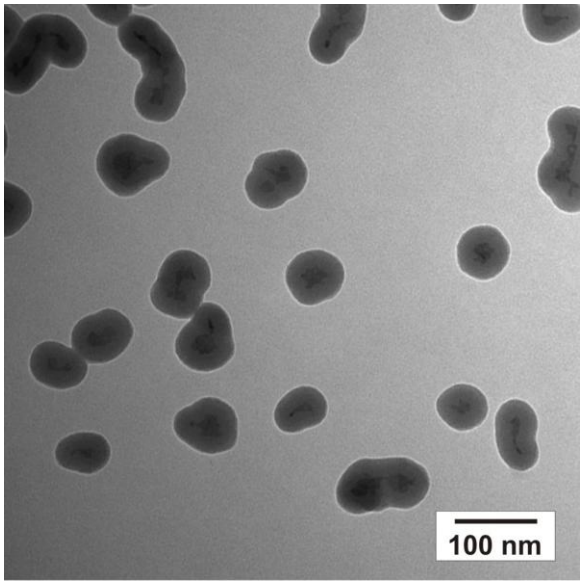

Figure 17: TEM of silica-coated particles after isolation.

Once the particles were isolated, they were annealed, as previously described, which changed the nature and appearance of the particles, eliminating enough quenching to allow upconversion to be detected.

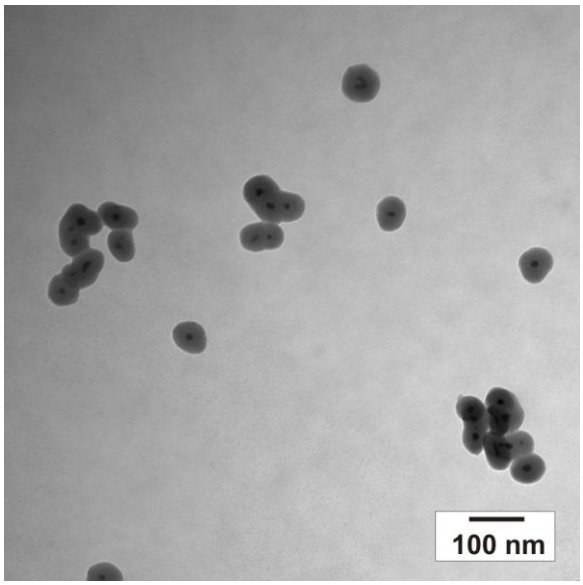

Figure 18: TEM of annealed silica-coated nanoparticles.

The exact change in nature of the particles is unknown because it depends on many variables such as drying, baking, and the quantity of TEOS used during the silica coating. However, our group has demonstrated, in the past, that under some circumstances silica-coated LaF_3 nanoparticles turns into a Ln^{3+}-doped $La_2Si_2O_7$ crystal phase[70] after baking. In this case, as shown in the XRD analysis section, some conditions lead to a Ln^{3+}-doped $La_{10}(SiO_4)_6O_3$ phase. The duration and high temperatures used for annealing pretty much guarantees the total elimination of water and removal[63] and a large majority of the OH groups, this assumption was supported by the dramatic decrease in quenching of the Tm^{3+} emission. It was also evident from the TEM of the annealed particles (Figure 18), when comparing it to the TEM of unbaked particles (Figure 17), that a significant change had occurred. The first interesting distinction can be observed in the core of the particles. It is as if they all had fused together to create a much more symmetrical center. Unfortunately, at that stage most of the particles were aggregated although the ones that were not looked very nice.

2.3.3. XRD of the silica-coated LaF_3 nanoparticles

More than only looking at the silica coating with TEM, the nature of the samples was also investigated. The silica coating before baking is not crystalline and therefore did not significantly affects the LaF_3 XRD pattern as shown by Figure 19.

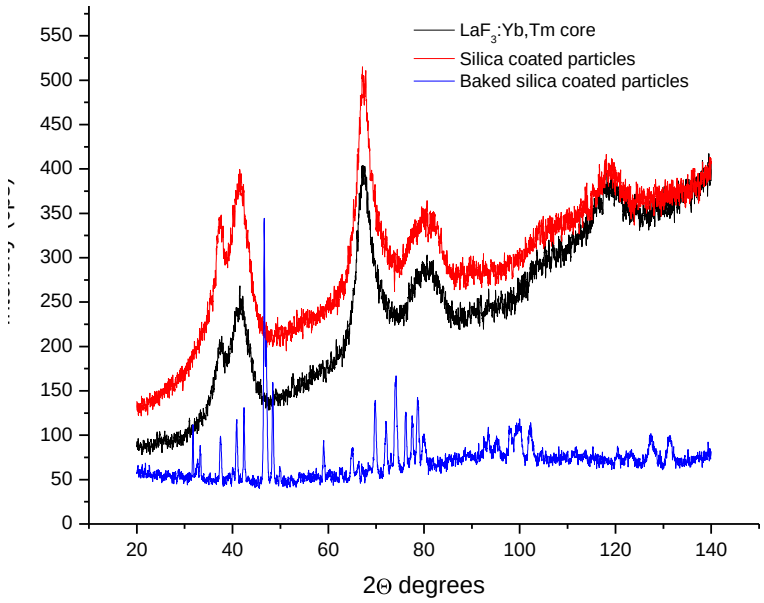

Figure 19: Comparison between the XRD during the three main stages of the synthesis of the desired nanoparticles when using 0.2 mL of TEOS. (Black and red lines shifted for clarity and backgrounds were not subtracted because increase in background sometimes indicates amorphous phases.)

The silica-coated pattern (the red line) in Figure 19 is therefore similar to the LaF_3 core pattern (the black line). As shown by the TEM images, a coating did occur and the upward shift in the low 2θ degrees region of the XRD is consistent with an amorphous, porous silica layer which is expected from the Stöber synthesis. On the other hand, a change in the pattern was always observed after baking the sample, but its nature depended on, among other things, the quantity of TEOS used during the synthesis. For example, when analyzing the XRD pattern of the annealed particles formed with 0.2 mL of TEOS, as shown in Figure 19 and Figure 20, it is possible to associate it with the reference pattern for lanthanum oxide silicate: $La_{10}(SiO_4)_6O_3$. However, even though the XRD gives the impression that there is only one crystal phase present, this is inconsistent with the TEM that clearly shows two compounds of different electron density which can be explained by a second phase of amorphous silica.

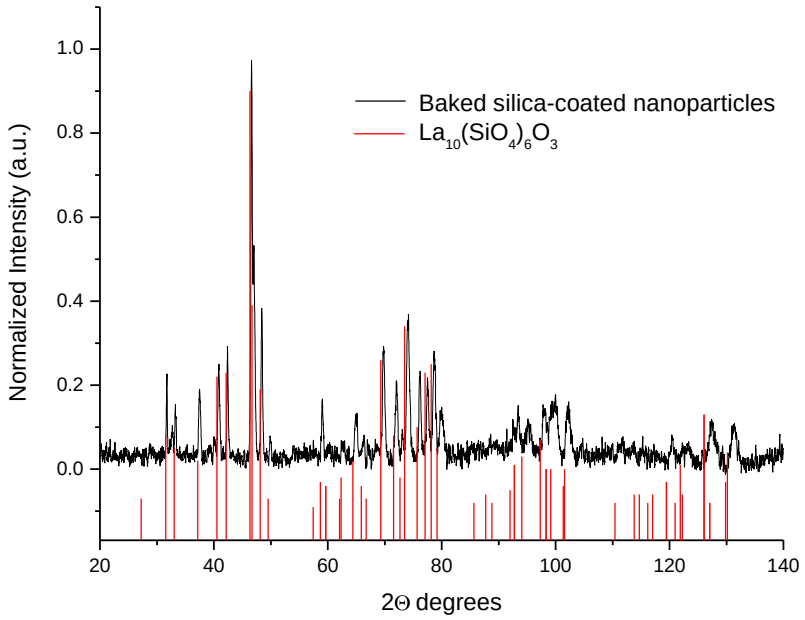

Figure 20: Example of a XRD pattern of baked silica-coated nanoparticles showing a lanthanum oxide silicate crystal structure: $La_{10}(SiO_4)_6O_3$ (PDF#00-053-0291).

Careful observation of the lanthanum oxide silicate pattern above shows a slight shift of the measured pattern compared with the reference lines of lanthanum oxide silicate. This was attributed to a small change in unit size caused by the doping in Yb^{3+} (0.98 Å) and Tm^{3+} (0.99 Å) ions which are smaller than La^{3+} (1.18 Å)[13]. As mentioned before, different results were obtained when using different quantities of TEOS in the synthesis. In this case, anything higher than 0.2 mL of TEOS lead to an XRD pattern that could not be assigned to a specific crystal structure because crystallinity decreased significantly with larger quantities of TEOS (Figure 21). These less crystalline XRD spectra can not be identified but they do not correspond to the lanthanum oxide silicate phase presented above nor do they fit with the fluorecite pattern (LaF_3).

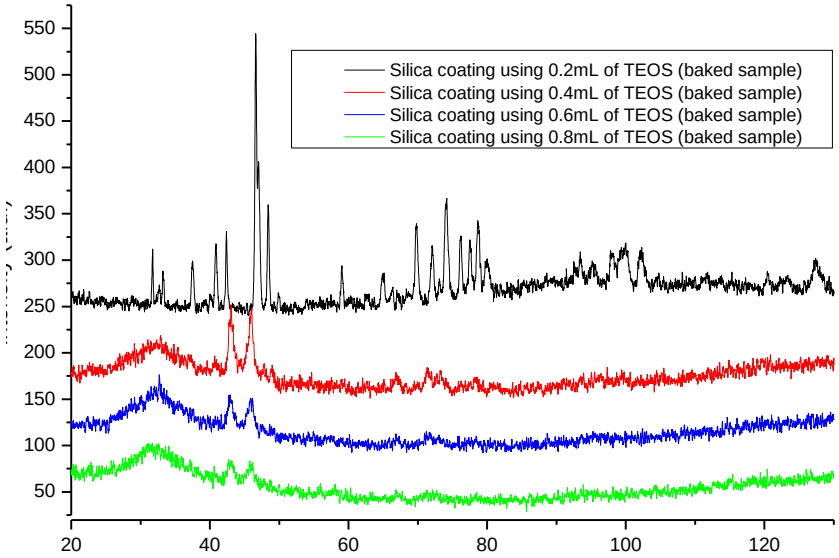

Figure 21: Comparison of XRD pattern for samples synthesized using an increasing quantity of TEOS. (Blue, red, and black lines shifted for clarity.)

They are however consistent with a range of silicon oxide phases so the most likely explanation for this (Figure 21) is that the core still changes into an unidentified crystal phase and is surrounded by amorphous SiO_2.

2.3.4. Upconversion

After annealing, the silica-coated nanoparticles exhibit upconversion. The two major emission peaks seen are 800 and 475 nm. The intensity of the 800 nm is, as expected, by far the most intense (Figure 22), because a two-photon process (see section 1.2) is far more likely to occur than a three-photon process.

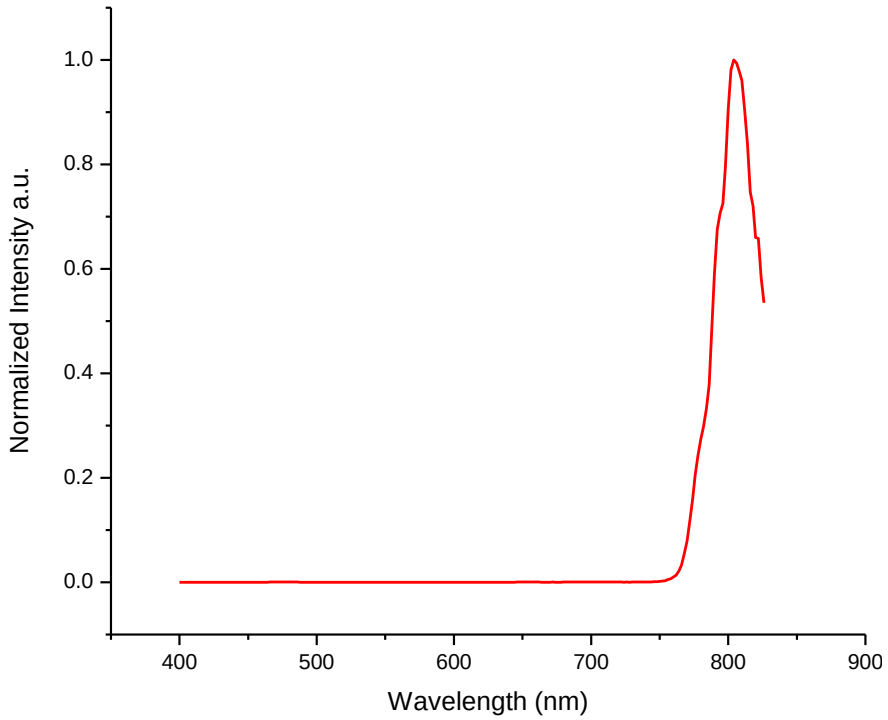

Figure 22: Upconversion at 800 nm from baked silica-coated LaF_3:Yb,Tm nanoparticles measured in a KBr pellet and excited with a 980 nm CW laser.

800 nm is within the near-infrared region, and cannot be seen by the human eye. On the other hand, the 475 nm emission (Figure 23), blue, can be seen when using an appropriate power density (at least few hundreds W/cm^2).

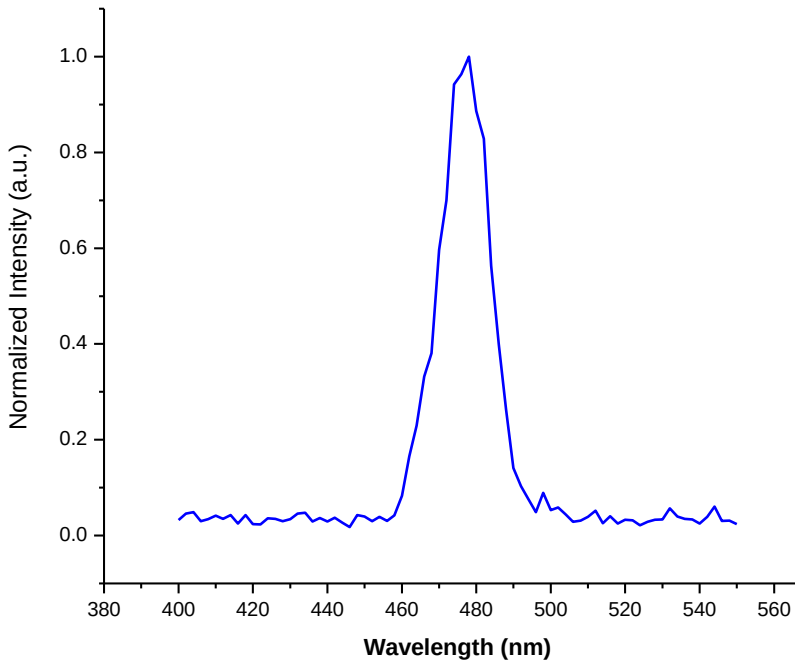

Figure 23: Upconversion at 475 nm from annealed silica-coated LaF_3:Yb,Tm nanoparticles measured in a KBr pellet and excited with a 980 nm CW laser (~ 200W/cm^2).

This emission is illustrated by the picture of a KBr pellet (Figure 24). It is important to mention that part of it might look white here but only as a result of an overexposure of the camera's CCD. The entire spot is in fact of the same color as the edges of the spot on the picture.

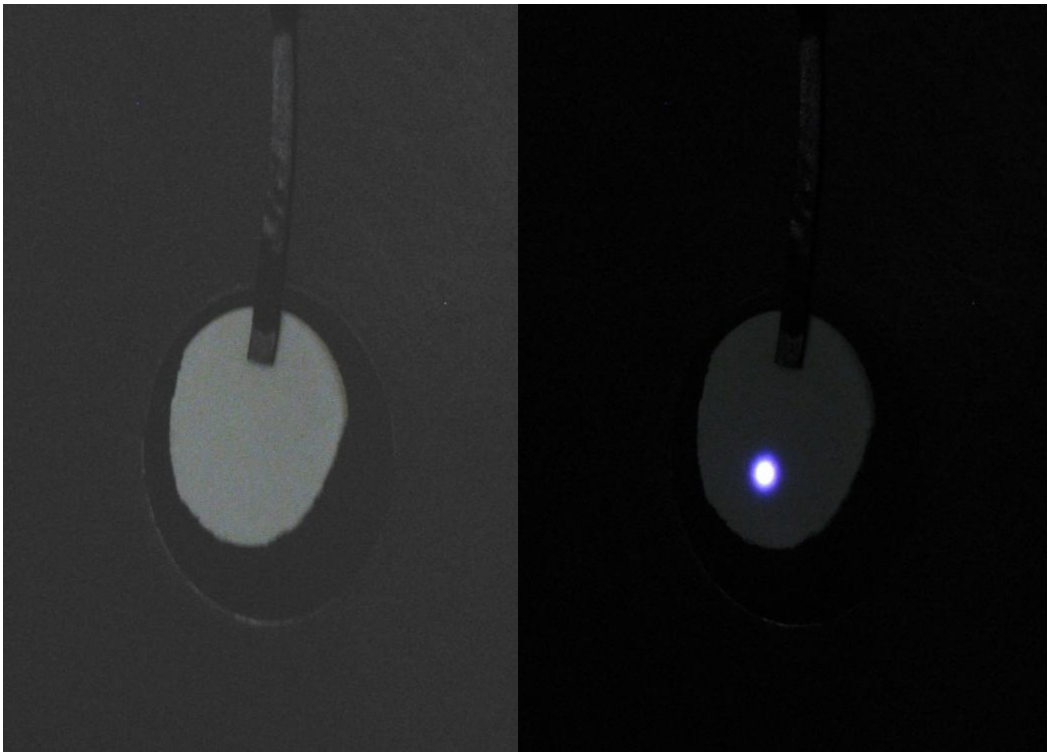

Figure 24: Picture of a KBr pellet containing baked silica-coated LaF_3:Yb,Tm nanoparticles showing blue upconversion at 475 nm when exciting with a 980 nmCW laser.

2.4. Obstacles

Due to the sensitivity of the upconversion to OH groups, the nanoparticles required an annealing. This resolved the quenching issue but, unfortunately, lead to aggregation and a considerable loss in dispersibility. Originally, the LaF_3:Yb,Tm citrate nanoparticles are easily dispersible in water, but for the silica-coated particles, there is already a significant loss in dispersion stability. The latter can normally be dispersed in ethanol at low concentration without too much difficulty, but the result is often slightly hazy. This depends highly on the quality and aggregation level of the particles but it is possible to obtain reasonable results. The main obstacles arose following the annealing step. As mentioned earlier, the nature of the particles changed substantially during this process and the particles lost the vast majority, if not all, of their OH groups. In any case, it does

lose all of its surface OH groups. This is exactly what is desired with respect to the improvement of the optical properties but it also means that the surface of the particles is now left without OH groups to interact with solvents like water or ethanol and create a uniform, stable dispersion. Unfortunately, the annealed particles behaved like small grains of sand and we were not able to obtain dispersions. It was attempted to use KOH etching to reactivate the surface of the particles. Adding KOH to the water did, in some cases, resulted in what seemed to be a clear dispersion but the particles were actually destroyed and intact nanoparticles could not be isolated.

2.5. Conclusion

In conclusion, the synthesis of silica-coated nanoparticles was achieved through a modified Stöber process on citrate stabilized LaF_3:Yb,Tm particles. The physical properties of these entities were monitored and encouraging results were obtained after some tuning of the silica coating procedure but the annealing step ended up generating other difficulties. It gave to the material its desired upconversion capabilities but it eliminated its dispersibility in water. Unfortunately, in the end, the KOH etching did not improve that aspect of the particles to allow the further modifications required to build a functional biolabel. Because the annealing seemed to be the step which complicated things, we then looked into slightly different systems who would not require any and decided to try to make some silica-coated $NaYF_4$:Yb,Tm nanoparticles, as presented in the next chapter.

Chapter 3: Second type of particles : $NaYF_4$ nanoparticles

3.1. Introduction

Considering that annealing was a significant obstacle we encountered during the first part of the project, we decided to turn to a different type of nanoparticles that would not require such heat treatment. We still wanted to exploit the same upconversion characteristics of a $Yb^{3+}$and Tm^{3+}system so what we needed was a different matrix to support these ions. We wanted a more efficient matrix that allows upconversion without further modifications and minimizes the effects of quenching on the emitting ions even in proximity of water. As mentioned before, bulk and nanosized materials doped with lanthanide ions have been studied by groups all around the world but one material retained our attention: sodium yttrium fluoride. In its hexagonal phase, the bulk material has been known as the best matrix[6, 40, 71] for upconversion for $Er^{3+}$and Tm^{3+} when codoped with Yb^{3+}due partly to its low phonon energies (between 300 and 400 cm^{-1})[6] but the specific mechanism leading to such improved luminescence properties is not known[71].

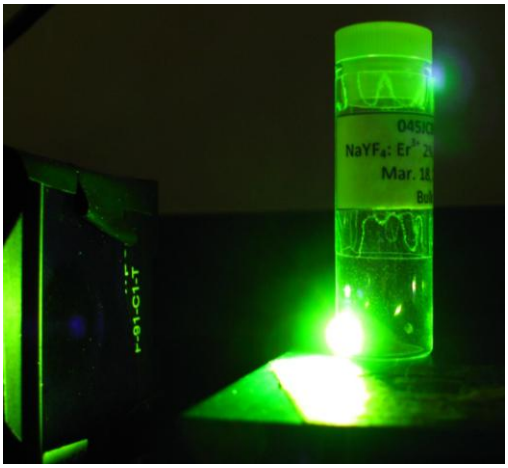

Figure 25: $NaYF_4$ is considered the best matrix for upconversion for Yb^{3+}/Er^{3+} and Yb^{3+}/Tm^{3+} systems. Here is an example of bright green upconversion from bulk $NaYF_4$:Yb,Er.

In light of all this, it seemed to be a good starting point, as others have shown[72], to develop a second type of nanoparticles. There are different ways to synthesized doped $NaYF_4$ nanoparticles but some[61, 73] of them lead to a material with a cubic phase, which is not as efficient as the hexagonal phase. An important drawback for the use of the particles as biolabel is that the most widespread synthetic routes[36, 40, 74, 75] in the literature for the production of nanoparticles having a hexagonal crystal structures involve an organic ligand, oleic acid, also frequently employ in the making of quantum dots[76]. Because of its use, the resulting nanoparticles are dispersible is organic solvent but not in water.

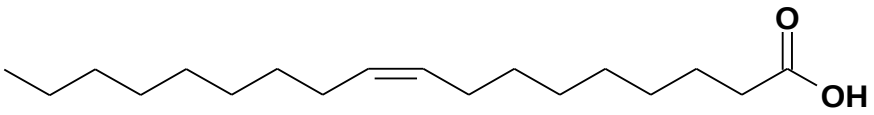

Figure 26: Chemical structure of oleic acid.

The challenge is then to modify the particles in order to obtain a water dispersible material that could be used in biological organisms. Different approaches to do so have

recently emerged of the literature, mainly divided in three groups: ligand exchanges, wrapping with polymers, or silica coating of the nanoparticles. As others[56, 77], we opted for the latter option because we believe that the encapsulation of the rare-earth metals in a silica shell is a significant advantage to minimize the toxicity of the nanoparticles. Some groups working on quantum dots already demonstrated[28] that it is an efficient way to reduce significantly the inherent toxicity of heavy metals for biological systems.

The second type of particles presented in this thesis is a silica-coated $NaYF_4$:Yb,Tm nanoparticle doped with 20% Yb^{3+} and 2% Tm^{3+}. The optical system exploited here is very similar to the LaF_3 based nanoparticles and the mechanism involved in the upconversion of 980 nm electromagnetic radiation into emission bands at 800 nm and 475 nm are the same as presented in the introduction of Chapter 2 (pages 21 and 22). The only difference here is that the new material allows upconversion to occur without further modification or annealing. As before, the matrix itself is optically inactive, it does not absorb or emit photons but puts the emitting ions in a favourable environment. The absence of that annealing step also simplifies significantly the further functionalization of the particles as their surface remains active compared to the inert glassy surface created by the heat treatment of the LaF_3 based nanoparticles. However, they will offer all the previously mentioned advantages (section 2.1) of a nanoparticles system over quantum dots and organic fluorophores.

3.2. $NaYF_4$ based particles synthesis

3.2.1. Experimental details

The following chemicals were used for the synthesis below. From Aldrich: thulium(III) acetate hydrate, 99.9%; ytterbium(III) acetate tetrahydrate, 99.9%; yttrium(III) acetate

hydrate, 99.9%; oleic acid, technical grade, 90%; 1-octadecene tech. 90%; ammonium fluoride, 99.99+% and Igepal CO-520. In addition, cyclohexane reagent ACS from ACP; anhydrous ethyl alcohol from Commercial Alcohols; tetraethoxysilane 99+% from Gelest and sodium oleate from TCI were used. Finally, ammonium hydroxide 28.0 to 30.0% NH_3 content, methanol HPLC grade and hexanes HPLC grade from Caledon were also used. These were all used as received, without further purification.

The centrifuge, sonicator, XRD, fluorimeter and TEM used were all the same as described in section 2.2.1. The same 980 nm CW diode laser from JDS Uniphase was used but it was powered at 2 A (~ 50 W/cm^2) by a programmable power supply PSP-2010 from GW Instek. During those measurements, again, the slits were opened for 1 nm resolution; a 850 nm low band pass filter (wavelengths shorter than 850 nm blocked) was put in front of the laser and a 800 nm high band pass (wavelengths longer than 800 nm blocked) filter before the monochromator. For the measurements on the core, one scan was performed and the dwell time used was 0.1 s; for the silica-coated particles, a dwell time of 0.2 s was used and 5 scans were performed for the 800 nm emission scans and 10 scans for the 475 nm emission scan. Again, the spectra of the 800 nm emission is cut at 825 nm because of the use of the 800 nm high pass filter.

3.2.2. Core $NaYF_4$:Yb,Tm synthesis

Different synthetic approaches can be used for the preparation of $NaYF_4$ nanoparticles but as mentioned before, it is important to obtain nanoparticles having an hexagonal crystal structure, which is more problematic. The core synthesis used is a modification of the one presented by Qian et al.[78] First, 0.78 mmol of $Y(OAc)_3$, 0.2 mmol of $Yb(OAc)_3$ and 0.02 mmol of $Tm(OAc)_3$ and 2.5 mmol of Na(oleate) were added to a 100 mL 3-neck

round bottom flask containing 10 mL of oleic acid and 10 mL of octadecene. Then, the mixture was heated up to 150 ºC under vacuum while stirring vigorously to dissolve everything. Once that was done, it was cooled back down to 50 ºC, after which a solution of 0.15 g of NH_4F in 10 mL of methanol was added dropwise. Finally, the mixture was heated up to 70 ºC until the methanol was evaporated, then up to 300 ºC under argon and was maintained at that temperature for 1.5 hours. The yellowish solution was cooled down to room temperature and precipitated with ethanol, centrifuged and washed with ethanol. The white precipitate was dissolved in 2 mL of hexanes, reprecipitated, centrifuged and washed with ethanol. Finally, it was dissolved in 10 mL of cyclohexane and the residues were let to settle overnight. The supernatant was then transferred to another vial and this was the final solution used for the silica coatings.

3.2.3. Silica coating of the nanoparticles

To coat these particles with silica, we used a modification of a procedure by the Han group in Singapore[79] on quantum dots: a microemulsion technique. Once again different experimental conditions were explored but here is a typical synthesis that gave good results. To 15 mL of cyclohexane add 1 mL of Igepal CO-520 and 0.25 mL of the $NaYF_4$:Yb,Tm particles cyclohexane solution (concentration of the solution was evaluated to be in the range of 3 wt%.) was added while stirring vigorously for at least 30 min between each additions.

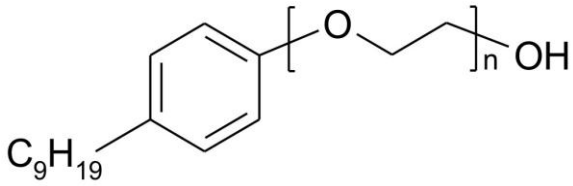

Figure 27: Chemical formula of Igepal CO-520, a surfactant used during the microemulsion for silica coating (M_n ~ 441, so n ~ 5).

Next, 50 μL of NH_4OH were added very slowly using a gauge 30 needle. Addition of bigger drops resulted in an irreversible precipitation of the core nanoparticles. Finally, after another half hour, 50 μL of TEOS were added. The emulsion was let to react for 24 hours. The regular precipitation procedure was to split the reaction mixture in two centrifuge tubes (30 mL) and fill them up with methanol to perturb the emulsion. These were centrifuged at 12000 rpm (12557 × *g*) for 10 min, washed twice with methanol and stored as a dispersion.

3.3. Results and discussion

$NaYF_4$ nanocrystals doped with 20% Yb^{3+} and 2% Tm^{3+} were synthesized at high temperature in octadecene in presence of oleic acid. These were then coated with silica using a microemulsion technique involving TEOS. The following section presents the different analysis performed on these particles.

3.3.1. Core analysis

The obtained $NaYF_4$:Yb,Tm, nanoparticles were white, with sometimes a yellow tint to them. This tint mostly likely came from overheating of the ligands and it was eventually minimized with a more careful control over the temperature. The core is readily dispersible in organic solvents like hexanes, cyclohexane, chloroform, dichloromethane

and most probably many others. It formed a clear and colourless solution with sometimes a slight yellow hue.

3.3.1.1. TEM

In opposition with the nanoparticles presented in the previous chapter, the size and shape of these $NaYF_4$ nanoparticles was more easily evaluated because a direct observation of the particles was possible using TEM. One of the micrographs taken is presented below. It was observed that the sample was not perfectly monodisperse but was composed of a reasonably narrow range of sizes. From a quick observation it seemed like all the particles had a diameter between 10 and 20 nm which was later supported by the XRD analysis (see section 3.3.1.2). Because optical characteristics of these particles are not governed by their size (unlike quantum dots) strict monodispersity is not an immediate requirement.

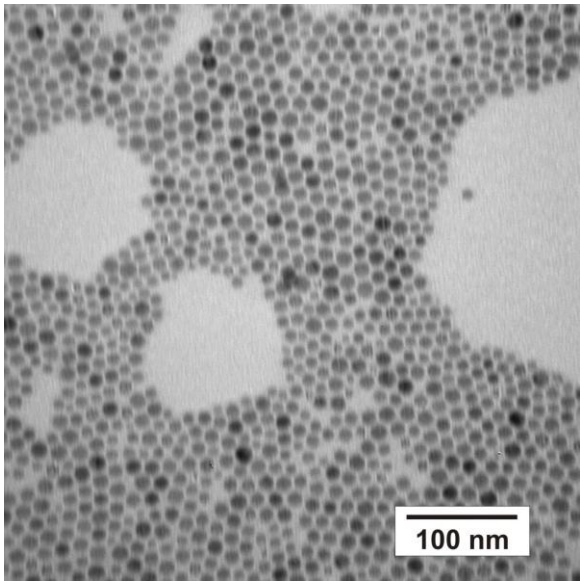

Figure 28: TEM of $NaYF_4$:Yb,Tm nanoparticles used as core.

3.3.1.2. XRD analysis of the $NaYF_4$:Yb,Tm core

As mentioned earlier, it has been observed by others that the hexagonal phase favours upconversion so it was important that the nanoparticles possessed that same characteristic. The hexagonal crystal structure of our nanoparticles was confirmed by the powder XRD analysis (Figure 29).

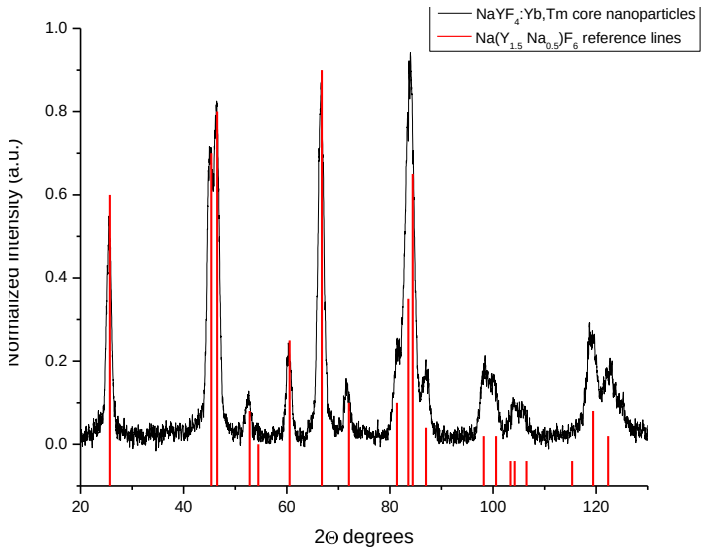

Figure 29: Example of a XRD pattern of $NaYF_4$:Yb,Tm core nanoparticles showing a hexagonal phase of $NaYF_4$ crystal phase: $Na(Y_{1.5}Na_{0.5})F_6$ (PDF#00-016-0334).

The notation $Na(Y_{1.5}Na_{0.5})F_6$ denotates that hexagonal phase of sodium yttrium fluoride and is used to differentiate from the cubic phase of $NaYF_4$ in the world of X-ray analysis, however, $NaYF_4$ is employed throughout this thesis for the sake of clarity. The broadening of the lines was again used to evaluate the crystallite size. The sizes always seemed to correlate well with TEM analysis and were estimated to be between 11 to 17 nm in this case.

3.3.1.3. Upconversion

The upconversion characteristics of these particles are very similar to what was presented before because one of the advantages of the lanthanides ions is their constancy with respect to their emission properties. The mechanisms involved were presented in section 2.1. However, one of the great advantages of these particles is that their upconversion is easily detected, even in a dispersion state and prior to any other modifications (no need for silica coating or annealing). Obviously, because the two-photon upconversion produces near-infrared radiation (800 nm) the only one observable is the three-photon process which gives out a nice blue light. Figure 30 shows the blue upconversion observed when passing a 980 nm CW laser beam through a cyclohexane dispersion containing some $NaYF_4$:Yb,Tm nanoparticles.

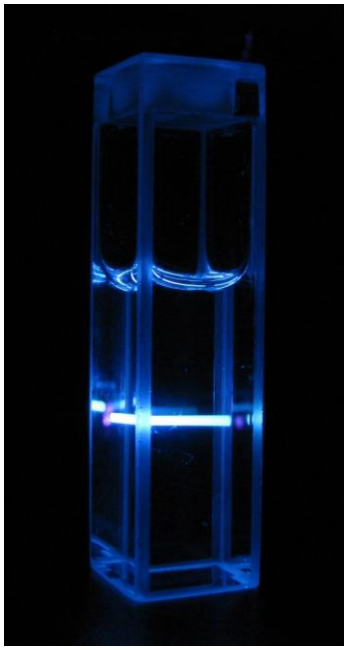

Figure 30: Picture of a dispersion in cyclohexane of $NaYF_4$:Yb,Tm nanoparticles showing blue upconversion at 475 nm when excited with a 980 nm CW laser (~ 200W/cm^2).

Once again, the white region in Figure 30 here is solely an artefact created by the overexposure of the camera CCD.

The upconversion from this dispersion was measured with a fluorimeter: the 800 nm emission (Figure 31) was once again much larger than any other peak which is perfect because it is the wavelength of most interest as it is within the biological window.

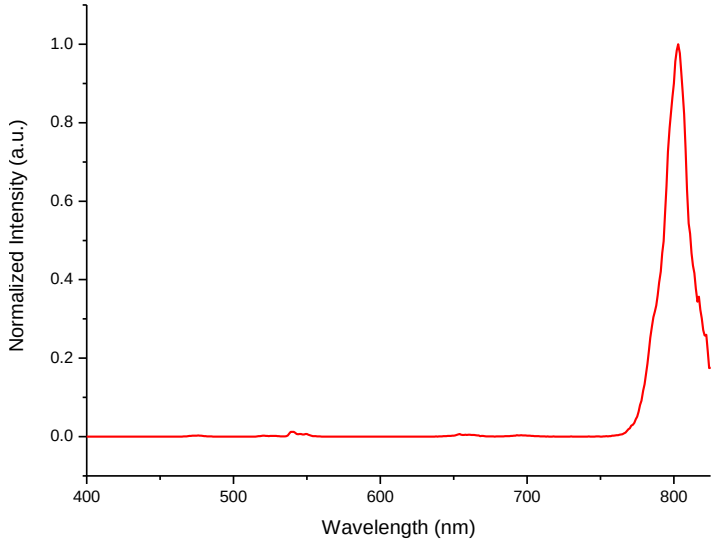

Figure 31: Upconversion at 800 nm from $NaYF_4$:Yb,Tm core Measured for a dispersion in cyclohexane and excited with a 980 nm CW laser.

As expected, the spectrum is very similar to the one observed before for the LaF_3 based nanoparticles. On the other hand, the spectrum of the blue emission showed one important discrepancy. Figure 32 shows the blue upconversion from Tm^{3+} (475 nm) but also includes a green peak (540 nm) not observed before (Figure 23).

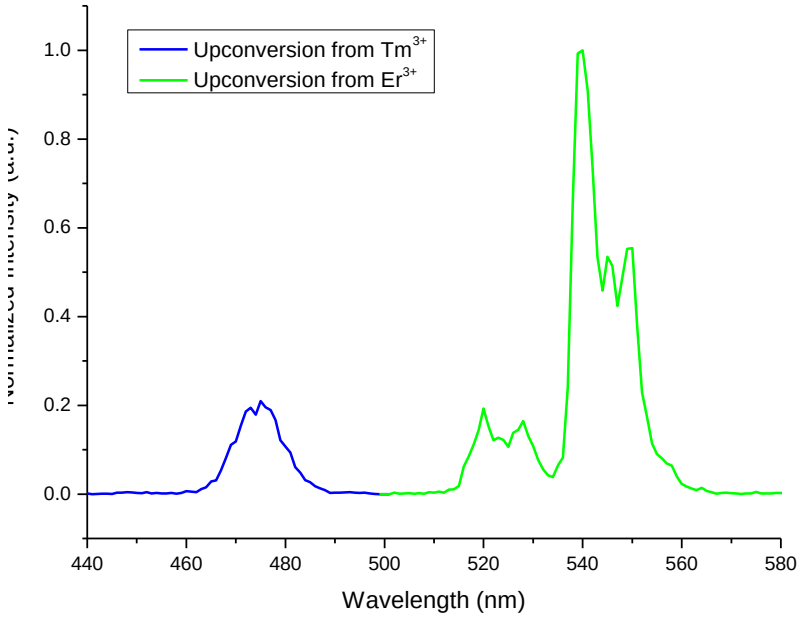

Figure 32: Upconversion at 475 nm (blue line) from core $NaYF_4$:Yb,Tm Measured for a dispersion in cyclohexane and excited with a 980 nm CW laser. The green (540 nm) indicates a slight contamination of the core with Er^{3+}.

Fortunately, there is an extremely simple explanation for this. It appears that the sample was contaminated with some Er^{3+}. Er^{3+} is well known for its efficient upconversion at 540 nm when in proximity of Yb^{3+} ions. From previous experiments done within our group[5], it seemed obvious that it was responsible for this extra peak observed in Figure 32. It is also known to be a contaminant in lanthanide salts and the certificate of analysis of the acetates used clearly specify that other rare-earth metals could be present. The green from $Er^{3+}$is a two-photon process that occurs as shown by Figure 33.

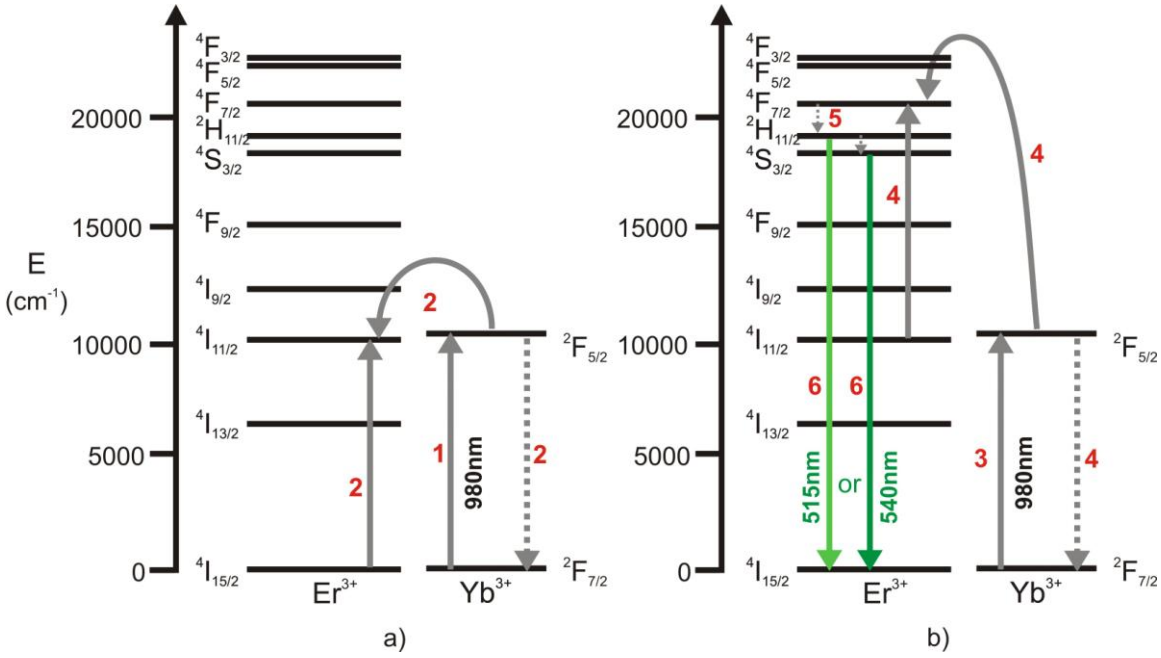

Figure 33: Mechanism[8] for green upconversion, among others, in an Er^{3+}, Yb^{3+} system.

First, an Yb^{3+} ion absorbs the 980 nm excitation beam and transfers its energy to a neighbouring Er^{3+} ion. Before it has time to relax down, another Yb^{3+} ion absorbs and transfers energy to this Er^{3+} ion to bring it all the way up to the $^4F_{7/2}$ excited state. Then it generally undergoes internal relaxation to $^2H_{11/2}$. From there, two emitting processes can occur to produce slightly different greens. The ion can either emit a 515 nm photon or it can relax down just a bit more to $^4S_{3/2}$ and from there emit a 540 nm photon.

However, the blue emission from Tm^{3+}comes from a three-photons process (Figure 10) so they should behave differently depending on the excitation power[6] A two-photon process is proportional to the square of the power density while a three-photon process is proportional to the cube of the power density of the excitation wavelength. Figure 34 shows that increasing the power of the excitation increases the 475 nm/540 nm intensity ratio. However, it was not safe for the fluorimeter to increase the power of the excitation laser enough to see the blue overcome the green emission.

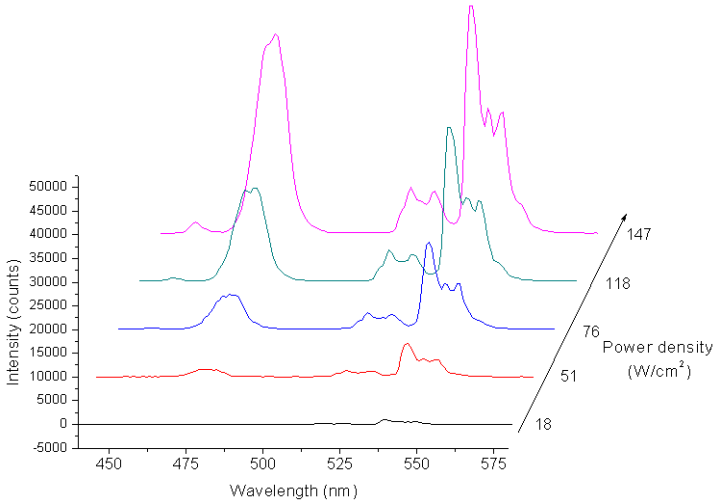

Figure 34: Power study showing the change in ratio with increasing power between the blue (475 nm) and the green (540 nm). Excitation power increases from front to back.

Figure 35 shows the relationship between the logs of the intensity of each peak and of the power density.

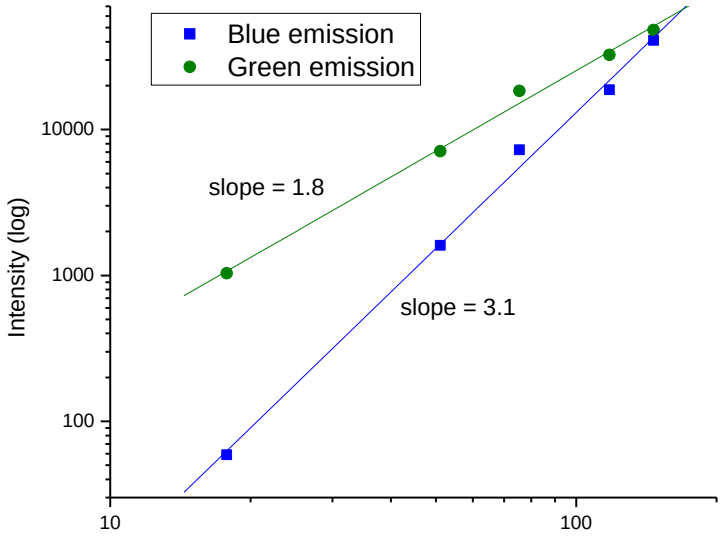

Figure 35: Power study of the emissions, blue (475 nm) and green (540 nm), from the $NaYF_4$:Yb,Tm nanoparticles showing contamination with Er^{3+}.

From the slopes it was calculated that the 475 nm emission comes from a three-photon process (slope = 3.1 ± 0.3) and that the 540 nm emission comes from a two-photon process (slope = 1.8 ± 0.2). This confirms the identity of the impurity present in the nanoparticles as being Er^{3+}. It also explains the presence of a small perturbation at around 650 nm in Figure 31 which is due to another two-photon emission from Er^{3+} as well. Because we are primarily interested with the 800 nm emission line, this is not a concern. Theoretically, this competitive upconversion probably reduces the efficiency of the process but the level of contamination is extremely low as can be seen in Figure 31. The 800 nm emission is about 100 times more intense than the 540 nm one; therefore this is not a real problem.

3.3.2. Silica coating analysis

Because the core nanoparticles prepared are stabilized with oleates, they were not dispersible in water or ethanol which eliminate the possibility of using the Stöber[68]

process as before (section 2.2.3). Therefore, a microemulsion in presence of TEOS was used to coat the nanoparticles. The reaction times were varied from 3 to 100 hours but the best results were obtained with 24 hours (as presented in experimental section). To get the particles out can be really difficult, in theory perfect particles would simply not precipitate, but the method presented above seemed to give good results. However, drying the particles is not advised because it can remove the solvation layer, which resulted in an aggregation increase and a dispersibility decrease.

After the silica coating procedure the obtained nanoparticles are most definitively white, but once again the samples are almost never dried completely to preserve their dispersibility. The obtained nanoparticles were dispersible in ethanol but the resulting dispersion was hazy, though stable. Unfortunately, dispersions in water were not stable.

3.3.2.1. TEM

To observe the nanoparticles, TEM was used once again because there was still an obvious contrast between the electron density of the $NaYF_4$ core and the silica layer. Different silica coating experimental conditions were tried and even if the microemulsion procedure is very different from the Stöber process used originally (section 2.2.3), the experience acquired then, proved to be useful here and it did not take as many trials to find conditions that worked well. The main issue encountered in this case was the inclusion of many cores inside one silica shell. Figure 36 is a good example of such problem.

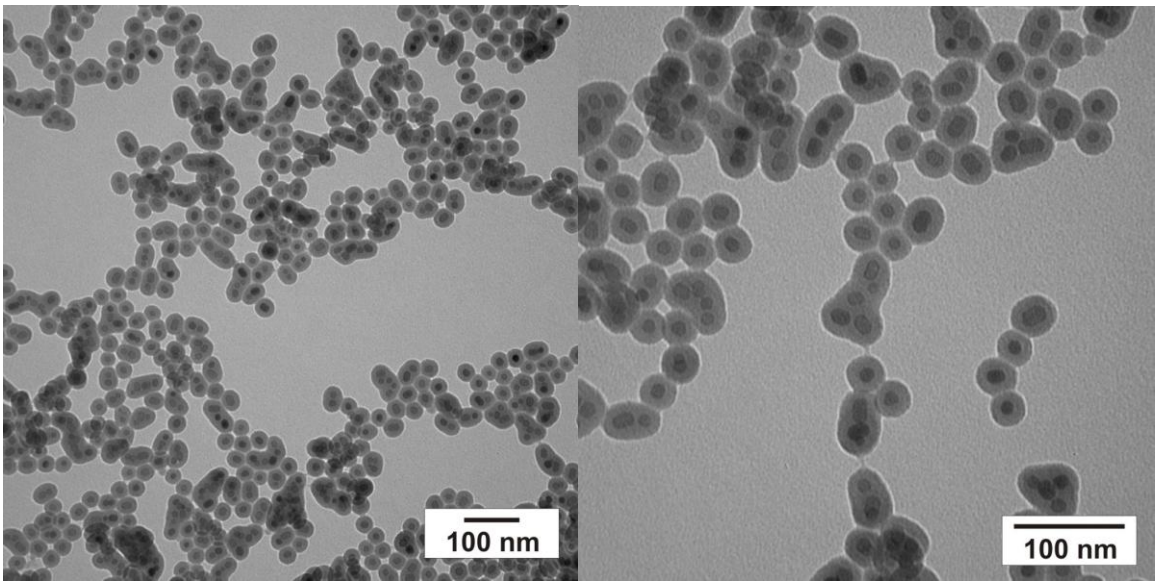

Figure 36: TEM of silica-coated particles where there were lots of silica shells containing more than one core.

It seems that this can be minimized by using a smaller amount of NH_4OH in the synthesis as illustrated by the following sample which was produced simultaneously, using the same method, but half the amount of ammonia.

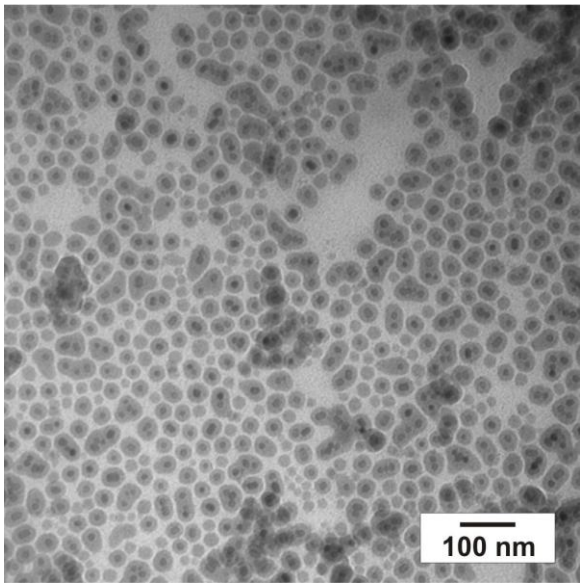

Figure 37: TEM of silica-coated nanoparticles presenting fewer instances of silica shells containing multiple cores, and less aggregates.

There are still some odd particles that contain more than one core but not that many. Aggregation is not completely eliminated either but it was deemed acceptable because approximately more than 80% of the particles were individual.

As mentioned earlier, drying leads to a lot of aggregation as shown by the sample below. It was let to dry before being redispersed in ethanol but the particles settled down quickly.

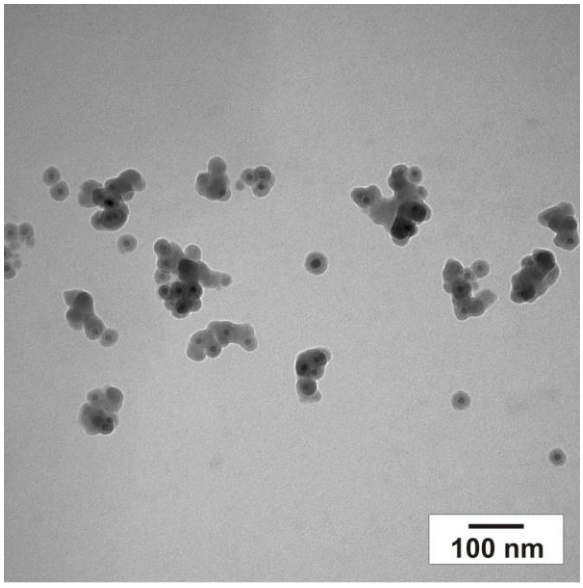

Figure 38: Example of aggregation of the silica-coated nanoparticles due to drying.

Thankfully, many samples exhibited overall good physical characteristics, as well as good dispersion stability in ethanol.

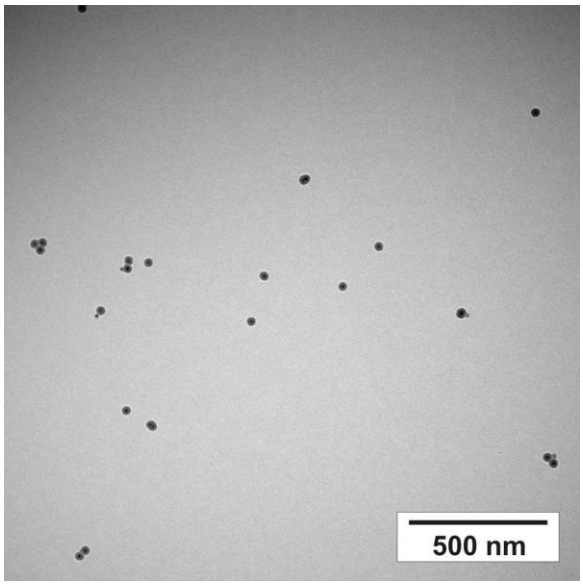

Figure 39: Example of nice silica-coated nanoparticles.

Once the physical appearance of the particles was established, their optical properties were also evaluated.

3.3.2.2. Upconversion

The upconversion of the particles was easily detected for dispersions in ethanol. This was a great step ahead of the lanthanum fluoride based nanoparticles because even without any heat treatment of these $NaYF_4$:Yb,Tm nanoparticles, the upconversion was strong enough to be detected even in a suspension containing OH groups.

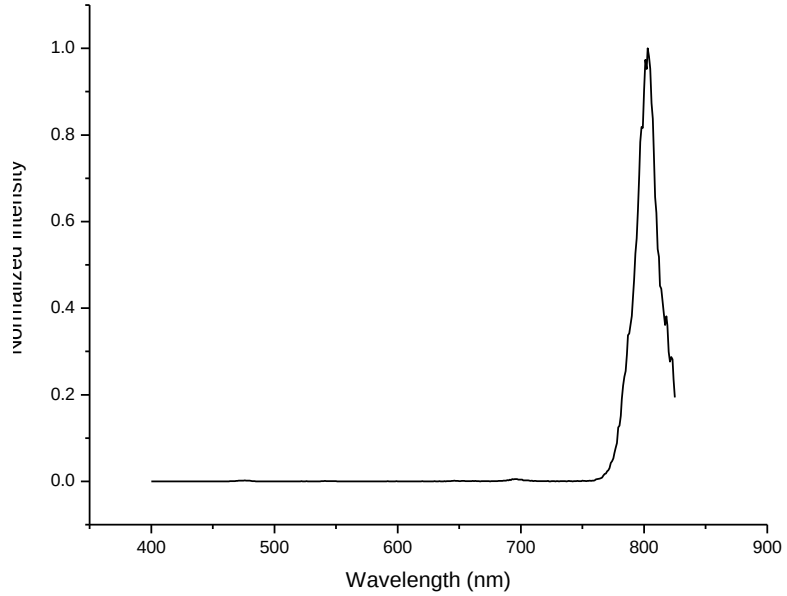

Figure 40: Upconversion at 800 nm from silica-coated $NaYF_4$:Yb,Tm Measured for a dispersion in ethanol and excited with a 980 nm CW laser.

To be noted that the rest of this thesis focuses solely on the 800 nm peak since it is the one of interest for imaging.

3.4. Conclusion

The $NaYF_4$:Yb,Tm nanoparticles are very promising but some issues still need to be addressed. The main concerns are aggregation and stability in water, and more specifically in phosphate buffers. The final objective is to be able to conjugate them to interesting receptors or antibodies for targeted imaging. To do so, most procedures of silica modification call for a functionality other than OH on the surface. The particles as they are right now schematically resemble this:

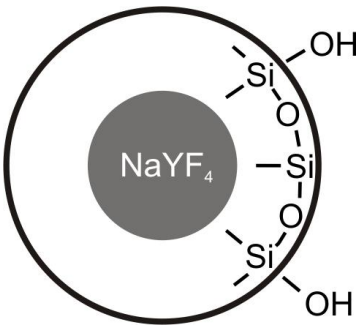

Figure 41: Schematic of the silica-coated nanoparticles.

The following chapter presents surface modifications of these nanoparticles and their incubation of cancer cells.

Chapter 4: Surface modification of the particles and imaging

4.1. Introduction

The silica-coated $NaYF_4$ nanoparticles presented earlier are very promising and were used to explore the biolabeling possibilities further. Eventually our group would like to able the functionalization of these particles with specific molecules like antibodies. For example, by putting cancer cell specific functionalities on particles, cancer cells could light up and ease their identification. In a general sense, bioconjugation in the literature goes through the use of functionalities like amines, thiols, carboxylic acids and maleimides: but rarely through OH groups which still allows chemical modifications. A lot of strategies are already in place so it was decided to take advantage of them. This explains the next step taken, the functionalization of the nanoparticles with NH_2 groups. This chemical handle could also be used to achieve another important objective: render the nanoparticles stable in an aqueous environment, and ultimately in biological fluids like growth medium or plasma. Unfortunately, stability in plasma is more complicated than stability in water for many colloidal systems because of the presence of a variety of species, chemical or biological, like ions or proteins. Lanthanide ions, for example, have a tendency to precipitate as phosphates and so do LaF_3 nanoparticles if they are stabilised with ligands that can be displaced by phosphate ions. A crude model often used in the lab to mimic problems with plasma is a phosphate buffer because these ions seem to be the source of a lot of problems with respect to stability. A compound commonly referred to as PEG (poly[ethylene glycol]) has been used to modify surfaces because it has been reported to[80]:

- render particles water dispersible

- give stability to particles in phosphate buffer
- prevent undesired protein adhesion
- be non-toxic
- be non-immunogenic
- delay opsonization
- improve biocompatibility

In light of this, the second step taken was to PEGylate the surface of the nanoparticles. The third step was to incubate ovarian cancer cells with these PEGylated nanoparticles and image them with a modified fluorescence microscope in order to determine if the particles penetrate the cell walls.

4.2. Experimental

4.2.1. Details for NH_2 funtionalization of the particles and PEGylation

The chemicals and the instruments used are the same as described in section 3.2.1. In addition to these, aminopropyltriethoxy-silane (APTES), 99% from Aldrich and ninhydrin from ICN were also used. In addition to these, 2-[methoxy(polyethyleneoxy)-propyl]trimethoxysilane, a PEGsilane from Gelest and m-dPEG$_8$-NHS from Quata BioDesign were used as PEG sources. The dimethyl sulfoxide (DMSO) came from Caledon while the *N*-(3-Dimethylaminopropyl)-*N′*-ethylcarbodiimide hydrochloride (EDC) came from Sigma.

4.2.2. Silica coating with APTES

The procedure developed in order to put NH_2 groups on the surface of the nanoparticles is simply a continuation of the silica coating experiment exposed in section 3.2.3. Three

hours after adding the TEOS to the microemulsion, a mixture of APTES and TEOS was added and let to react for another 24 hours.

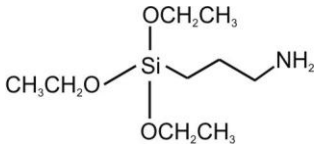

Figure 42: Chemical formula of (3-aminopropyl)triethoxysilane : APTES.

The best results in terms of the low aggregation and well-defined nanoparticles were obtained using 100μL of a 1:10 APTES:TEOS and the isolation of the particles was done exactly in the same fashion as exposed for the TEOS-only silica coating procedure (see page 45).

4.2.3. Silica coating with PEGsilane

The first PEGylation procedure was also a continuation of the silica coating experiment exposed in section 3.2.3. So in this case, three hours after adding the TEOS to the microemulsion, a mixture of the PEGsilane and TEOS was added and let to react for 20 hours.

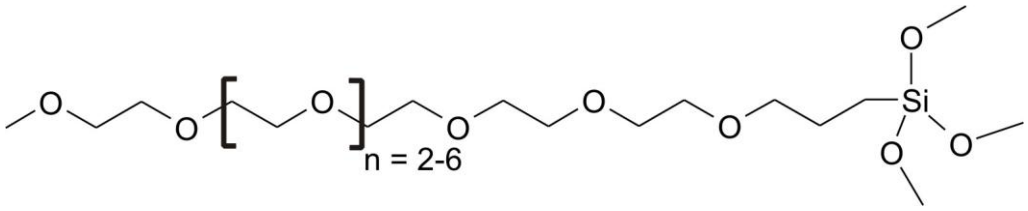

Figure 43: Chemical formula of the PEGsilane used. M_W = 450 to 600, 6 to 10 ethylene oxide units.

The best results in terms of dispersibility were obtained using 75μL of a 1:10 PEGsilane:TEOS and the isolation of the particles was performed as before (see page 45).

The particles were stored with 5 mL of 1:1 MeOH : PBS buffer. That concentration is too high to allow a good dispersion but keeps the particles well hydrated.

4.2.4. Reacting the NH_2 groups with mPEG-NHS

A dispersion of NH_2-modifed nanoparticles in water that had settled down was shaken to disperse them temporarily and 3 mL were taken, centrifuged, and washed once with DMSO. To the solid residues, 0.5 mL of DMSO were added and sonicated for 15 min. To this, 1 mg of EDC and 13μL of mPEG-NHS were added and stirred for 3 hrs after which 1 mL of MeOH was added. They were then centrifuged at 12 000 rpm (13 201 × g), washed with MeOH and PBS buffer and redispersed in PBS buffer.

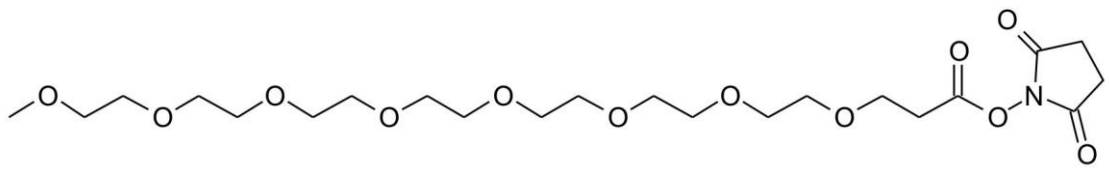

Figure 44: Chemical formula of the $mPEG_8$-NHS.

4.2.5. Ninhydrin test

About 1.5 mL of nanoparticles dispersions was centrifuged and the ethanol removed to obtain wet nanoparticles at the bottom of an epi tube (about 3 mm high). To this, were added 3 drops of 5 wt % ninhydrin solution in ethanol, which is yellow. The samples were heated on a bath at 70 ºC for 10 minutes.

4.2.6. Details for cell culture experiments

All the culture work was conducted at the Denley Research Centre (DRC) located at the Royal Jubilee Hospital in Victoria BC. The cell line chosen was a human ovarian cancer cell line identified as CaOV3, and was provided by the DRC. The cultures were grown using the 100 mm × 20 mm CELLBIND® surface dishes from CORNING and DMEM/

High glucose medium from HyClone enriched with 10 % FBS. Medium was a liquid containing appropriate amount of nutrients, amino acids, proteins and salts necessary to cell growth. The 0.05% Trypsin and the fetal bovine serum (FBS) used were also bought from HyClone while the trypan blue came from Sigma. All the cell culture work was performed following sterile techniques in the sterile environment of a Class II-B1 biosafety cabinets (BSC). For incubating the cells, 6 wells plates (6 well cell culture cluster flat with lid tissue culture treated, non pyrogenic, polystyrene, sterile) came from Costar and the quartz disc (1" diameter, 1/16" thick) from Technical Glass Products, Inc. Cell viability was tested using Tryptan solution (0.4 %) from Sigma.

4.2.7. Cell cultures

From frozen stock, the cells were suspended in about 13 mL of medium in a petri dish and let to attach to the dish and grow for 3 days. Once the culture was started, it was split about twice a week to a ratio depending on the growth but always close to a 1:5 ratio. These CaOV3 cells adhere strongly to the surface of the dish so the splitting was done as follow. First, the medium was pipetted and thrown away. The cells, attached to the dish, were washed with 5 mL of PBS buffer to remove residual medium. This is an essential step because Trypsin, an enzyme that will detach cells from the surface, is inactivated by the proteins contained in medium. Then, about 2 mL of Trypsin was added and let to act in an incubator at 37 ºC and 5 % CO_2. After 10 min of digestion, the majority of the cells were floating. However, some might still be attached, so the dish is rinsed with 5 mL of fresh medium, pipetting up and down to force the cells to detach from the surface. The resulting suspension of cells in medium was then centrifuged at 1200 rpm (311 × g) for 5 min at 4 ºC. This forced all the cells at the bottom of the flask so the medium containing

inactivated Trypsin was thrown away. After tapping the centrifuge tube to detach the cells, they were suspended in media to allow splitting. As mentioned earlier, the most often used splitting ratio was 1:5, so the cells were suspended in 5 mL of medium and after thorough mixing through pipetting, 1 mL was extracted and added to a petri dish containing 12 mL of fresh medium. The same dish was used 3 times before using a brand new one. Once the cells were in the dish, they were let to attach and grow for 3 to 4 days in an incubator at 37 ºC and 5 % CO_2. This was repeated about twice a week to prevent the cells from dying, from either running out of food or space.

4.2.8. Incubating cells with nanoparticles

In order to do imaging, the cells had to be fixed to a quartz slide so the incubation went as follow. One petri dish containing cells was treated with Trypsin as mentioned before to detach the cells from its surface. These were centrifuged and resuspended in 5 mL of medium. Using a calibrated counting chamber the number of cells per millilitre was estimated and different amount of cells were added to 6 wells plates at the bottom of which a quartz disc had been placed. The total amount of medium was adjusted to 2 mL in each well (just enough to cover the quartz slide). The cells were allowed to attach to the discs and grow for about 24 hours in the incubator and 37 ºC and 5 % CO_2. Once they were ready, the medium was removed and replaced by various amounts (see Table 3) of a suspension of nanoparticles in PBS buffer for 20 min. Then, medium was added to obtain a total volume of 2 mL and the cells where let in the incubator for about 24 hours. The following day, the cells were fixed in the following fashion. The medium was removed from all the wells and 5 mL of PBS was added to each well to rinse the discs. Pipetting up and down across the surfaces of the discs was used to ensure removal

of nanoparticles that would not be inside cells. Each disc was then put in a bath of PBS for 30 seconds, then in a well (6 wells plate) containing 10% formalin PBS solution for 15 minutes. From that bath, it was transferred into a second PBS bath for 30 seconds, followed by a quick rinse in a distilled water bath for about 10 seconds. Each baths contained about 20 mL of liquid. The discs were then extensively dried with a rapid stream of air, transferred in a new 6 wells plate for transport and finally stored in a dessicator at the university awaiting imaging.

4.2.9. Imaging details and method

Imaging was performed on a custom built microscope originally designed to perform Raman scatter measurements. It was built by Quinn Matthews in Andrew Jirasek's group at the University of Victoria. The CW laser is the same that as been used for fluorescence measurements (see section 2.2.1).

Figure 45 shows the excitation path. First the 980 nm laser line is guided through a 850 nm filter, then a neutral density filter wheel which was set to a 0 % filter then through a series of lenses that act as a collimator to focus the beam. After reflecting on two mirrors, it then reflects on a high band pass 840 nm filter which is graded as reflecting anything above 840 nm. From there, it enters the microscope and goes through the objective all the way to the sample.

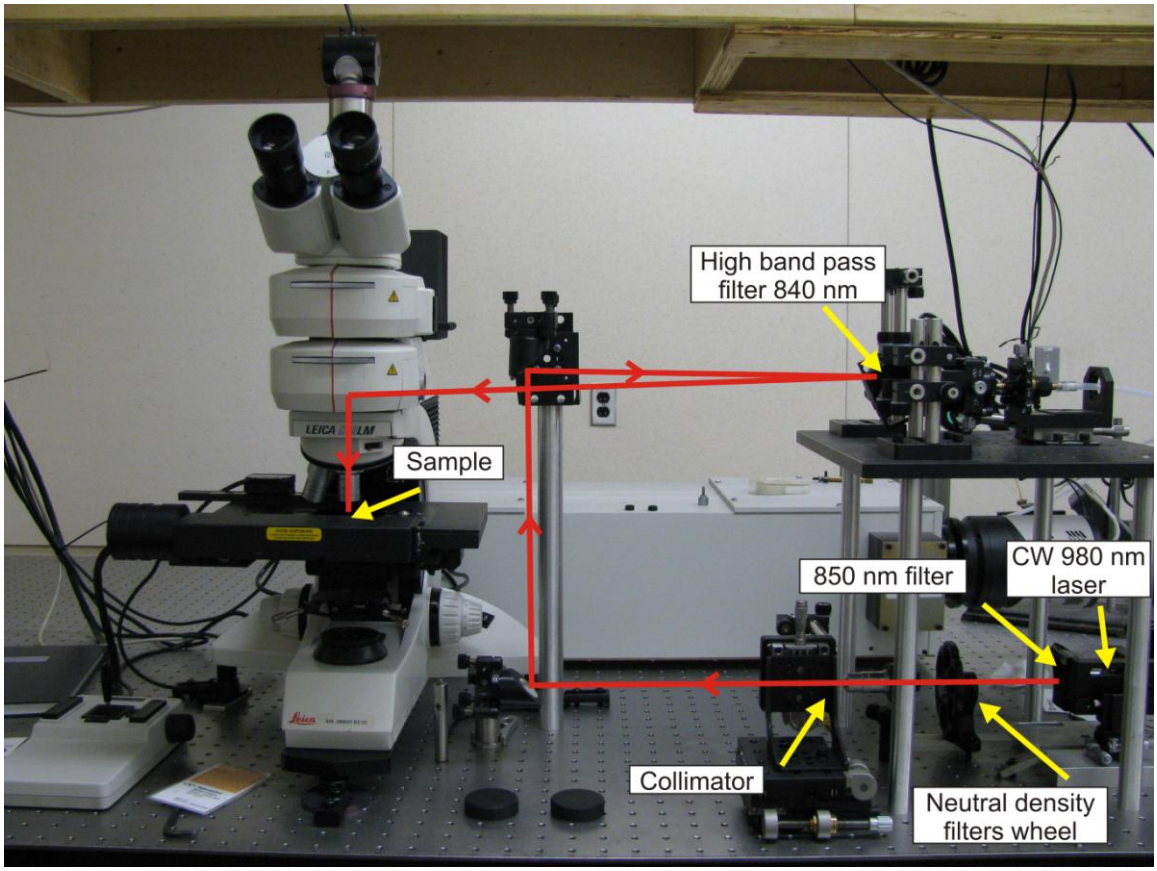

Figure 45: Excitation path of the microscope used for imaging.

The next figure (Figure 46) illustrates what happens to the emitted radiation as well as the scatter from the excitation beam. From the sample, luminescence goes through the objective and out of the side of the microscope, then through the high band pass filter (wavelengths longer than 840 nm blocked, reflected) into the fiber optic leading to the monochromator towards the detector. The microscope used was a LEICA *DMLM*, the monochromator was SpectraPro 2750 (0.750m Triple Grating Monochromator) from Acton Research Corporation and the detector was a PIXIS 400 from Princeton Instruments. The system is also equipped with a Renishaw RGH22 electronically controlled stage and a SPC 900NC PC camera from Philips that allows the user to take pictures as well as an electronically controlled stage that allows the acquisition of maps.

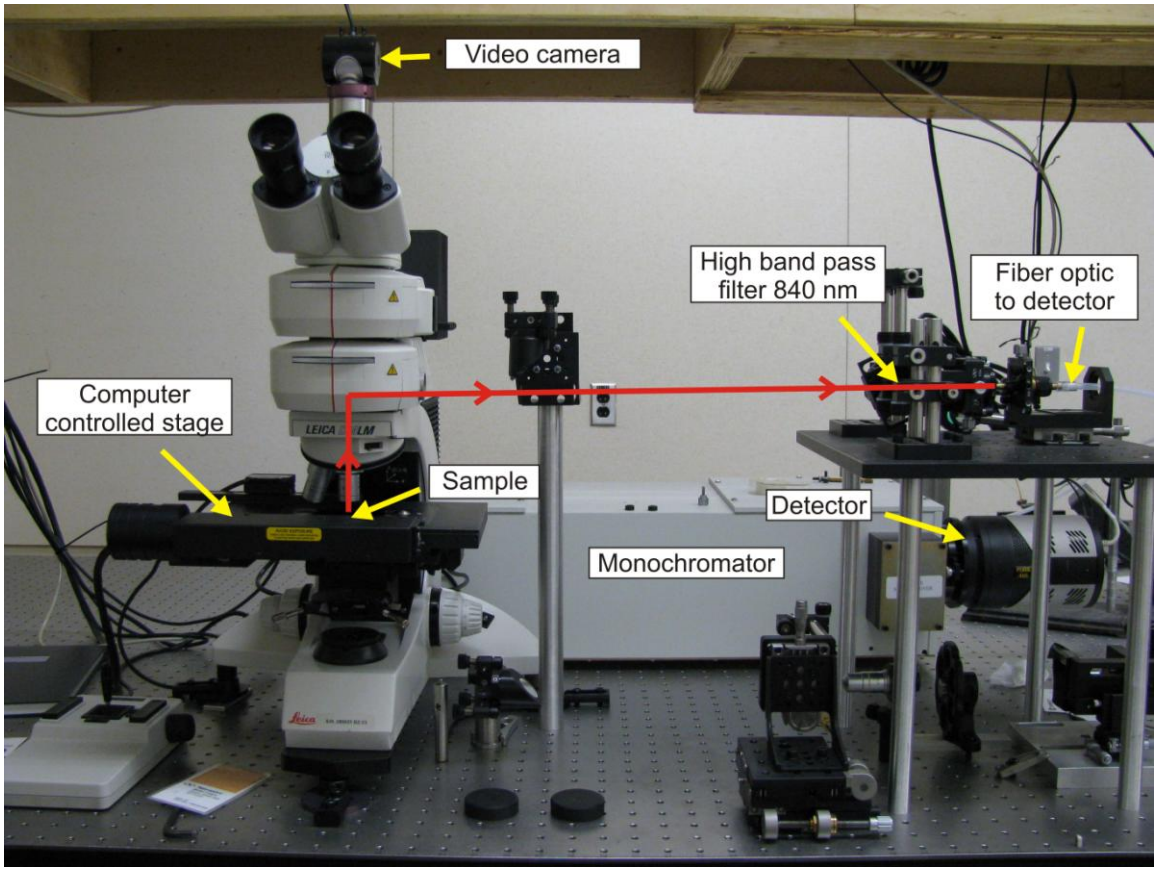

Figure 46: Emission path of the microscope used for imaging.

The program WinSpec/32 (version 2.5.19.0) from Roper Scientific was used to control the temperature of the detector (set to -75 ºC), Monochromator Control Software SpectraPro Version 3.33 was used to control the monochromator and Wire3.0 from Renishaw was used to acquire date and coordinate, camera, stage and detector.

The CW laser was set at 2 A (3.2 W) which led to a power density of the order of 10^5 W/cm^2 with the 50x objective.

The quartz discs supporting the cells were placed in a custom-built support to fit in the microscope to be able to place them on the microscope stage. Before taking a measurement of the luminescence at one location, a picture was taken where the data was

collected exactly in the center of that picture. All the spectra shown were measured using the 50x objective and an integration time of 30 seconds.

The maps were taken using the 50x objective, 3 μm steps, and the integration time was adjusted in function of the strength of the signal (see individual maps for the numbers). The colour coding was established as a function of the area under the curve between around 775 and 825 nm.

4.3. Results and Discussion

4.3.1. First step: NH_2 funtionalization of the particles

After silica coating, the surface of our nanoparticles is composed of OH groups[81], which, as mentioned before, is not typically used for biofunctionalization, so we decided to incorporate some NH_2 groups on the surface of our silica-coated particles. Alkoxysilanes containing amino groups are readily available and it has been shown to be a good strategy by other groups[21] so we opted for it instead of thiols, which are also easily available. The objective was to obtain a particle having some NH_2 groups on the surface and we expected something like Figure 47.

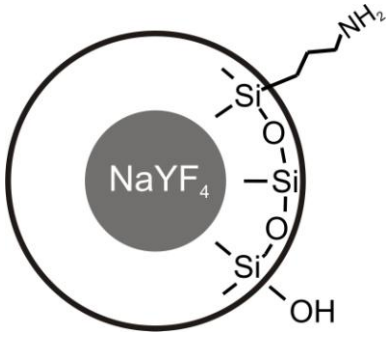

Figure 47: Schematic representation of the desired silica-coated nanoparticles functionalized with NH_2 groups.

The nanoparticles were modified by taking the silica coating procedure one step further to minimize isolation steps that seemed to reduce the quality of the particles and diminish dispersibility. A mixture of APTES and TEOS was added to the microemulsion described for silica coating for an entire day.

4.3.1.1. TEM

The few encountered problems were similar in nature to the ones presented in the previous chapter but the experience acquired during the last procedure helped tremendously to speed up the elaboration of the final procedure presented above.

For example some samples contained empty silica beads as shown here in Figure 48.

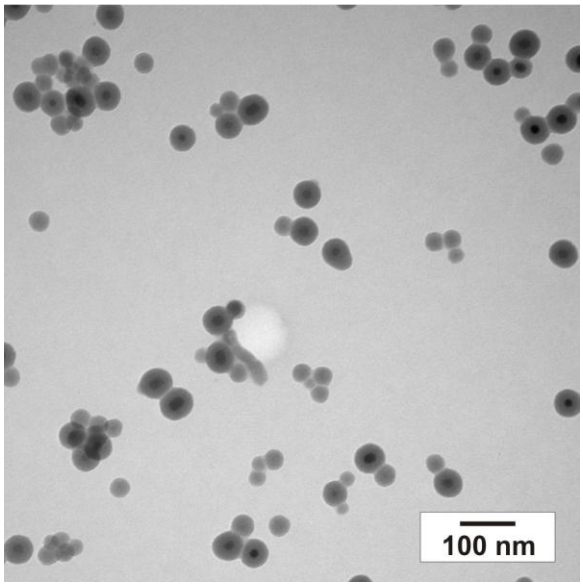

Figure 48: Example of a TEM of a silica-coated (TEOS and APTES) nanoparticles showing lots of empty silica beads.

However, diluting the reaction mixture to the conditions specified in the experimental section gave much better results as presented below in Figure 49.

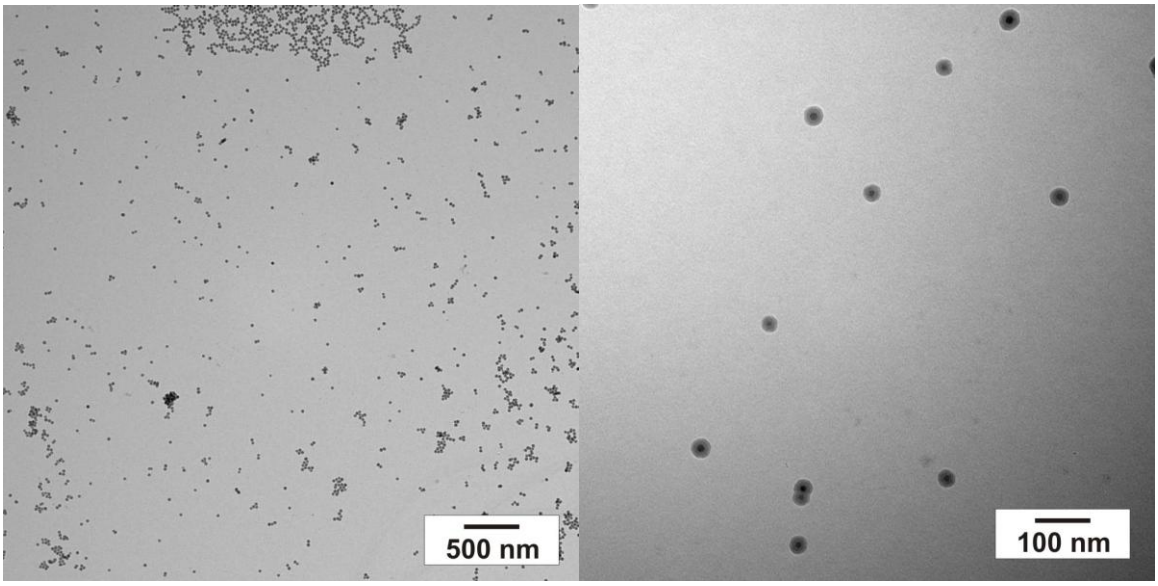

Figure 49: TEM of well defined $NaYF_4$:Yb,Tm single nanoparticles silica-coated with TEOS and APTES.

4.3.1.2. Dispersibility

Dispersibility of the silica-coated particles is hard to quantify because drying affects the samples significantly but when avoiding excessive drying, all samples dispersed readily in ethanol. Unfortunately the samples were not stable in phosphate buffer at pH 7.2 but dispersion in acidic water (pH 2.0) was possible, most probably because of the presence of amino groups on the surface of the particles which were protonated.

4.3.1.3. Upconversion

As with the silica-coated samples presented in Chapter 3, the upconversion is still visible in this case, as expected. The typical upconversion spectrum was measured for a suspension of the particles in ethanol (Figure 50) and in acidic water (Figure 51).

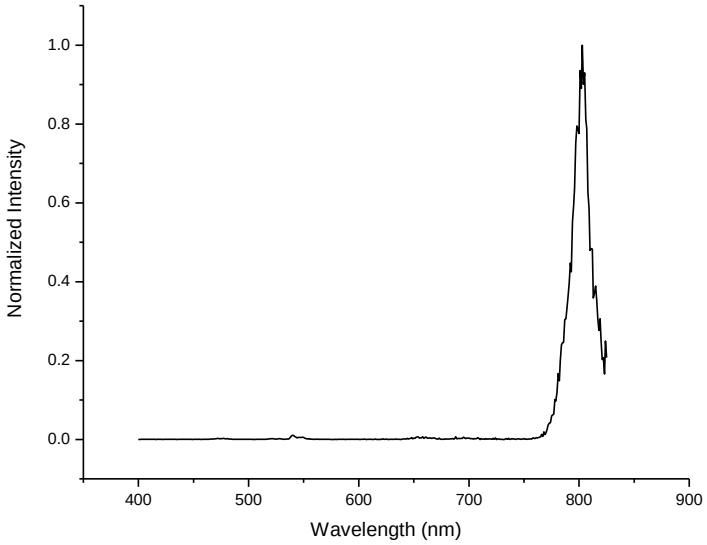

Figure 50: Upconversion spectra of APTES+TEOS coated nanoparticles dispersed in ethanol. The origin of the small peaks in the baseline is discussed in section 3.3.1.3.

This is an important step and proves that even in water, the upconversion is not completely quenched. This demonstrate the superiority of these particles when compared to the LaF_3-based nanoparticles (Chapter 2) because no annealing was required, and upconversion could be detected in a water dispersion, two things that were impossible before.

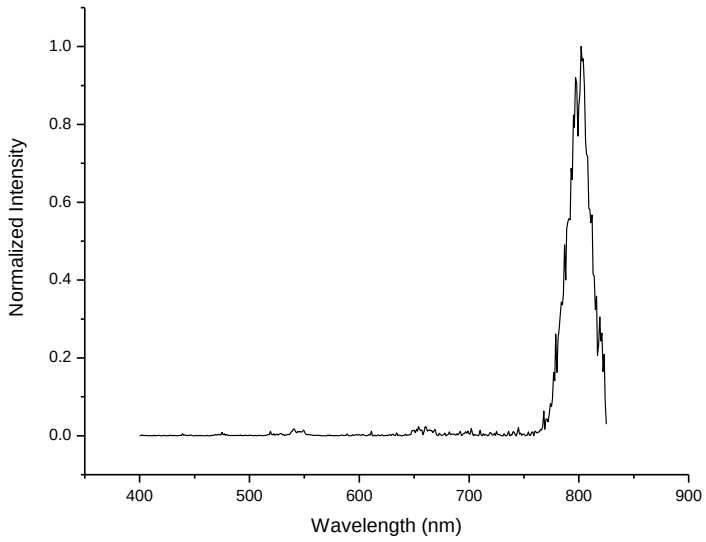

Figure 51: Upconversion spectra of APTES+TEOS coated nanoparticles dispersed in acidic water (pH 2) The origin of the small peaks in the baseline is discussed in section 3.3.1.3.

The noise is more obvious in the last two spectra shown because all the scans were taken with the same dwell time and scan repetition but at much lower concentrations.

4.3.1.4. Ninhydrin test

In order to confirm the presence of NH_2 groups on the surface of the nanoparticles, a chemical test was performed. Ninhydrin, is known to react with NH_2 groups to form a blue compound and has been used by others[82] to detect them on silica surfaces. All the sample silica coated with APTES turned blue rapidly whereas the ones synthesised with TEOS only did not.

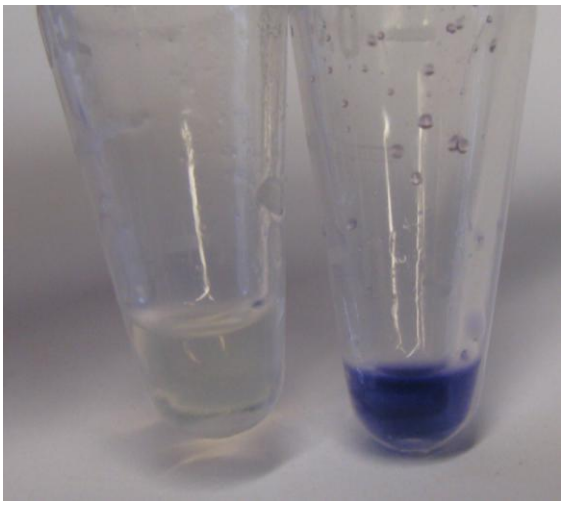

Figure 52: Comparision of ninhydrin test results between nanoparticles silica coated with APTES (RHS) or not (LHS).

Figure 52 shows the result of a ninhydrin test and confirms that NH_2 functionalization was achieved when using APTES.

4.3.2. Second step: PEGylation

As mentioned in the introduction, PEGylation offers a lot of advantages, including improvement of dispersibility in phosphate buffer, so two different ways to PEGylate the particles were explored. The first one using a PEGsilane, is very similar to the NH_2 method presented above because it is also a continuation of the silica coating procedure. The second one, using mPEG-NHS is a reaction where the NH_2 functionalized particles were the starting point.

Unfortunately only the first method led to a stable dispersion in phosphate buffer. In the second case, either the reaction did not occur or the PEGylation was not extensive enough to stabilize the nanoparticles. A ninhydrin test performed on the second type of nanoparticles after PEGylation suggests that a reaction did occur because the NH_2 could not be detected anymore but more experiments would be required to confirm this.

Because the best results were obtained with the first method, the following results focus on it.

4.3.2.1. Dispersibility

As mentioned above, stable nanoparticles dispersions were obtained only from the first PEGylated method. The dispersion was not 100 % clear but it was stable for over a day before showing any sign of settlements. After a week, a bit of residues accumulated at the bottom but they can be redisperse easily by vigorous shaking. This strongly suggests the presence of PEGs on the surface of the nanoparticles.

4.3.2.2. TEM

Some TEM were taken of a stable dispersion of the nanoparticles in PBS buffer, unfortunately the quality of the images is poor. This is most likely due to the presence of a lot of salts from the buffer and some residuals from the microemulsion, some surfactant and PEGsilanes from the silica coating procedure for example. However, some nanoparticles are easily distinguishable and considering that there was no time to optimize the conditions the results are very encouraging. No aggregation of the nanoparticles was observed but many of them (about half) contained more than one core (see Figure 53).

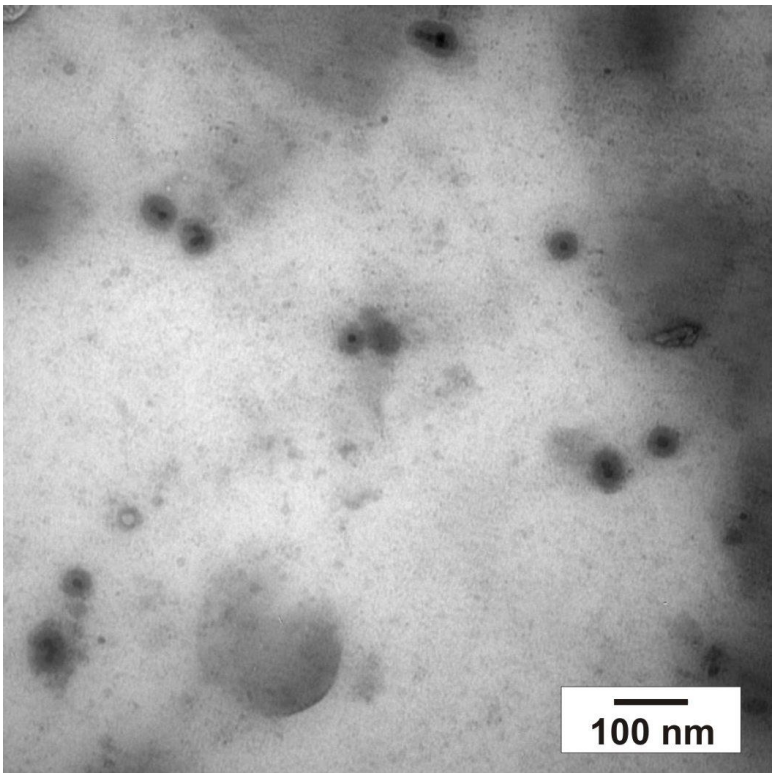

Figure 53: TEM of some PEGylated nanoparticles, a lot of residues are visible because the TEM was done of a suspension in PBS buffer.

Still, a lot of individual nanoparticles were seen and a closer look shows a blurry layer around each of them which suggests the presence of a PEG layer. Silica-coated nanoparticles normally have a very-defined edge (Figure 36) which indicates the possibility of a nature change in this case however it is important to mention that this is not a proof. TEM cannot confirm the nature of what seems to be an outer shell of less dense material around each individual particles (Figure 54) but it supports that hypothesis.

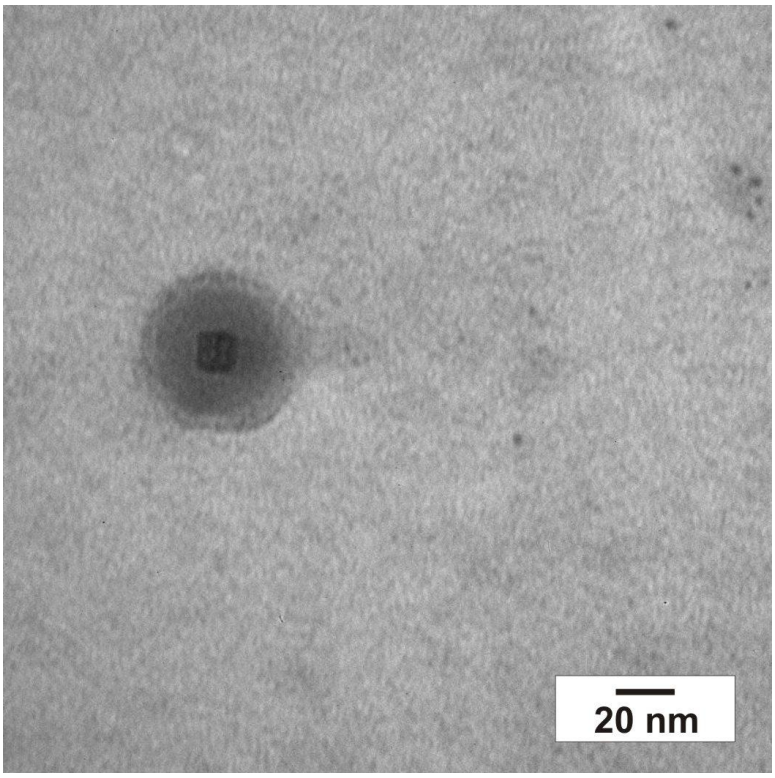

Figure 54: TEM of one PEGylated nanoparticle where a blurry layer, possibly a PEG layer, is visible.

However, more analyses are required to confirm this, for example with IR spectroscopy or NMR analysis. These were then used to incubate cells and do some imaging.

4.3.3. Third Step: Incubating cells with particles and Imaging

Once nanoparticles were obtained that were stable in buffer solution, it was decided to test them against live cells and see if it was possible to detect luminescence from cells incubated with the $NaYF_4$:Yb,Tm PEG silica coated nanoparticles.

Ovarian cancer cells (CaOV3) were cultured in petri dish for weeks at ther DRC of Victoria to prepare for some experiments to see the interaction of the nanoparticles with biological material. Figure 55 shows a cell culture, after growing for 1 day (LHS) and 6 days (RHS).

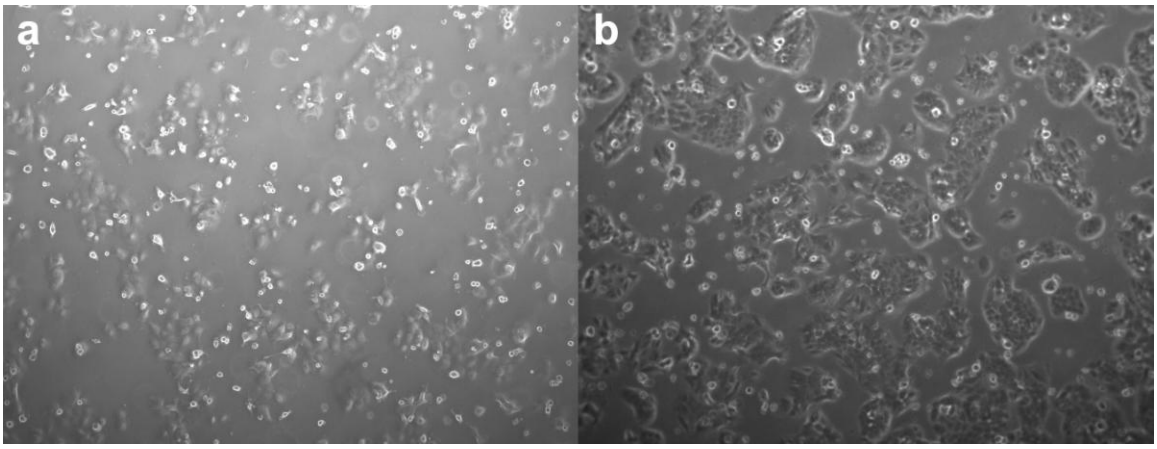

Figure 55 : Ovarian cancer cell (CaOV3) culture. a : 1 day growth, b: 6 days growth. Cells are around 40 μm in diameter.

Then, some of these cells were grown on quartz discs in the presence of PEGylated $NaYF_4$:Yb,Tm nanoparticles and these discs were then scanned with a custom made fluorescence microscope with, as the excitation source, a CW 980 nm diode laser.

Four different quartz slides were prepared, as shown in the table below.

Table 3: Quantities used for preparation of quartz discs to image incubated cells.

Quartz disc ID	Amount of cells (-)	Amount of nanoparticle dispersion (mL)
01cMP09	170 000	1
02cMP09	340 000	1
03cMP09	680 000	1
04cMP09	340 000	0.5

After incubation, a lot of cell debris has observed. This indicates that some cells died but this is more likely due to the use only half the medium required in a typical cell growth environment. This came from the fact that the nanoparticles were dispersed in PBS buffer instead of growth medium. In retrospective, growth medium would be a much better choice and will be used in the future. However, the bottom of the wells, where a

lot of cells had also grown, were tested with Tryptan blue and this indicated that a lot of the cells survived to these harsh conditions.

All four samples exhibited the typical 800 nm emission of the $NaYF_4$:Yb,Tm nanoparticles at position corresponding with numerous cells. The next figure shows an example of a cell where luminescence could be detected.

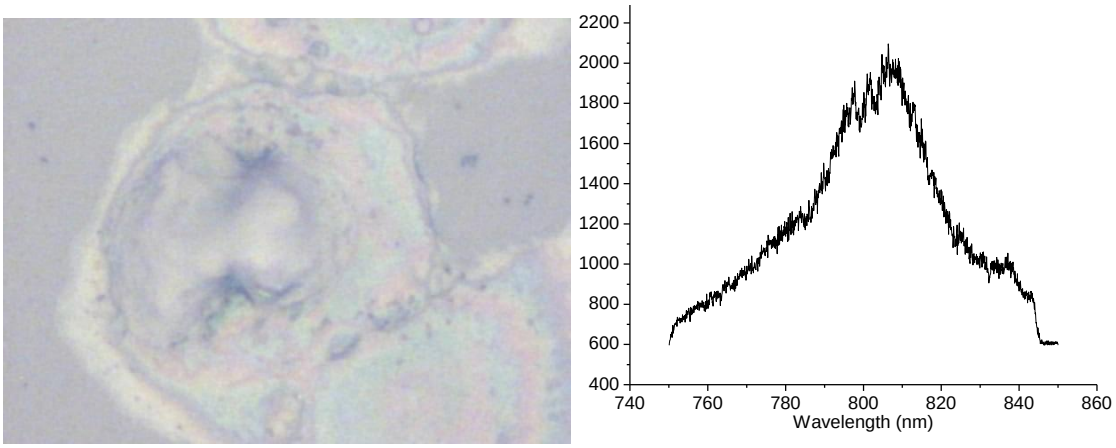

Figure 56: Upconversion measured in the centre of a cell (LHS) where the x-axis ranges approximately from 750 to 850 nm (RHS).

However, some cells did not seem to exhibit luminescence although this could be only due the exact point chosen to measure since this spectrum was taken only at the exact centre of the image.

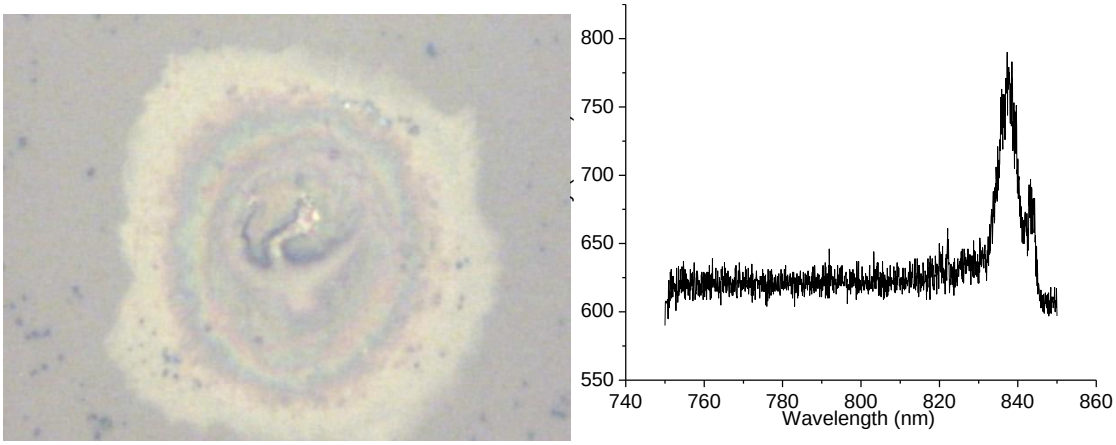

Figure 57: A cell not exhibiting any upconversion only an artifact is visible.

The luminescence spectra acquired with this system all possess an artefact around 840 nm but its origin is unknown. To study the distribution of the nanoparticles in the cells, some maps, as the one shown below, were taken.

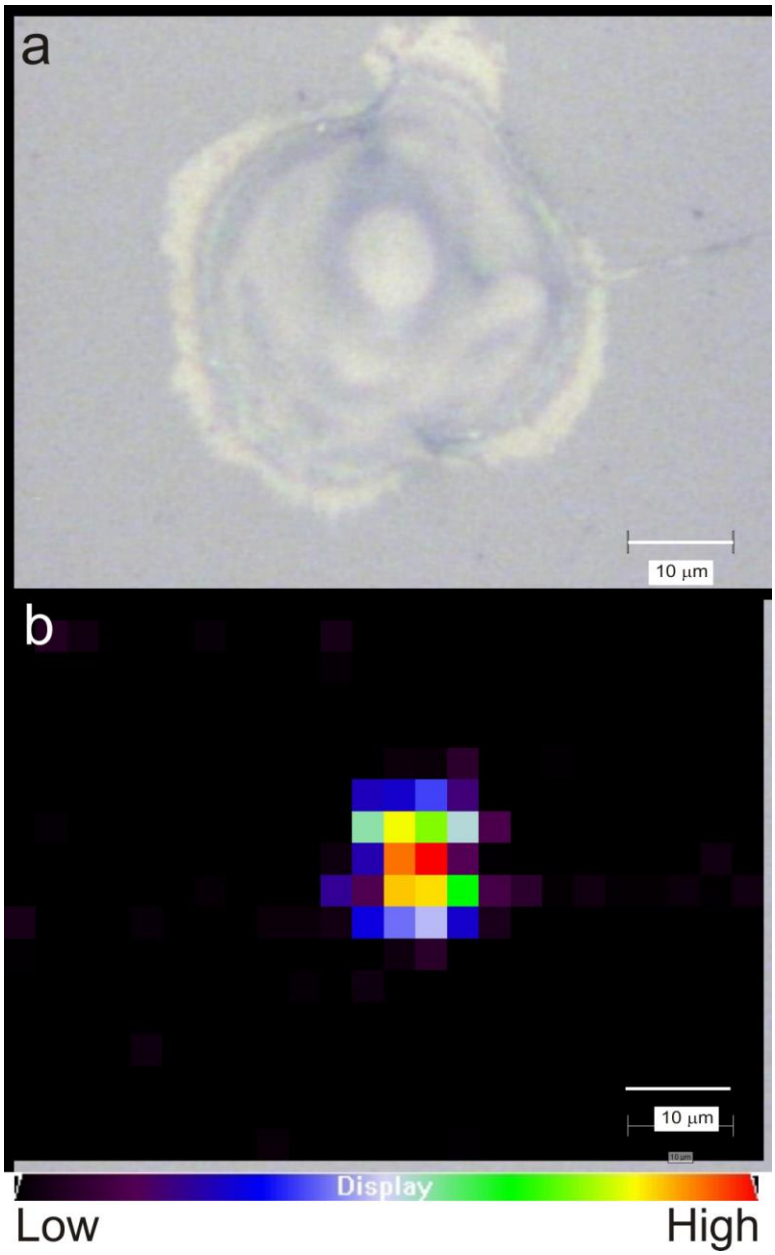

Figure 58 : Mapping of the luminescence ovarian cancer cell incubated with the PEGylated nanoparticles. a: optical image of the cell, b: position and intensity of the luminescence measured.

In all four samples a lot of small particles can be seen around the cells and it is still unclear what their nature is. The two most likely possibilities are cell debris or nanoparticles aggregates. Some do seem to exhibit luminescence but because of poor lateral resolution it is not possible to confirm them as particles, even more so that it is hard to comprehend their adhesion to the surface of the quartz discs. Another extremely curious phenomenon is this empty space around almost each cell. Figure 59 shows this phenomenon along with a map of the luminescence associated with this cell.

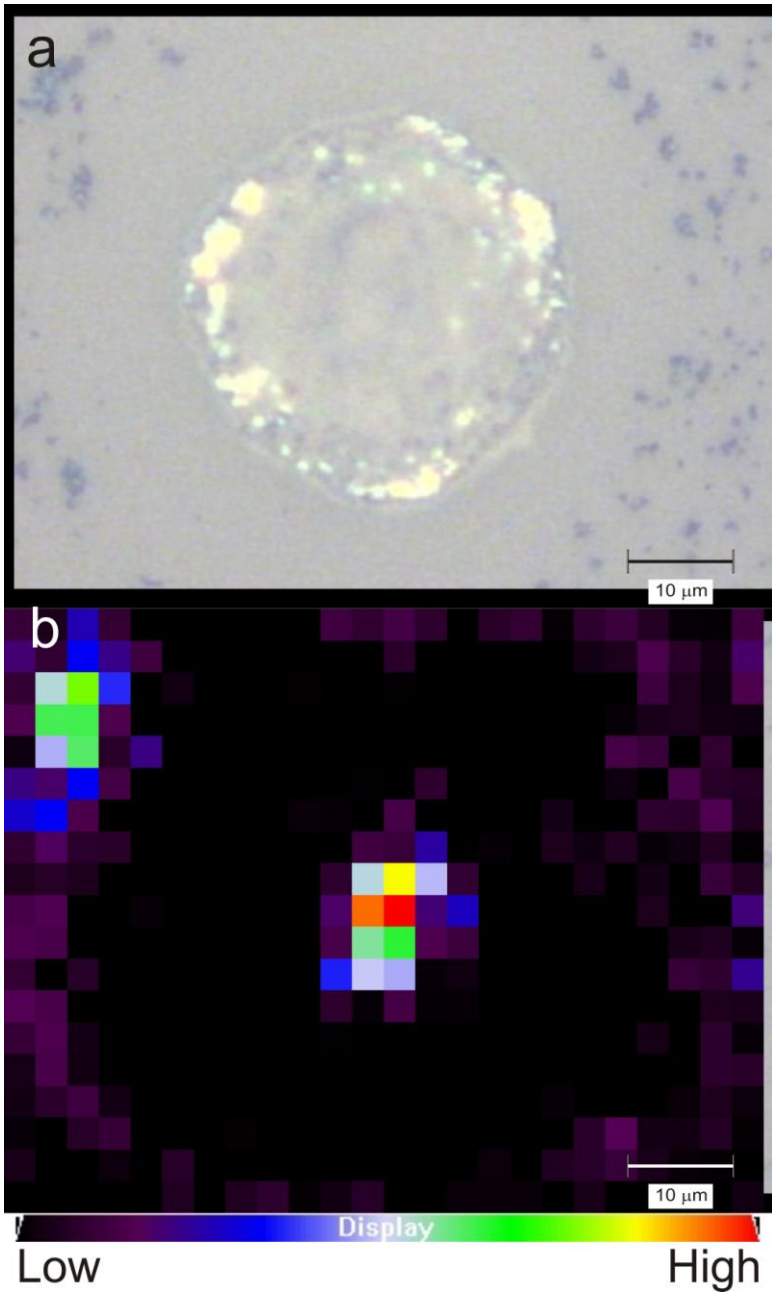

Figure 59: Mapping of the luminescence ovarian cancer cell incubated with the PEGylated nanoparticles. a: optical image of the cell showing particles around the cell, b: position and intensity of the luminescence measured.

Clearly, in this case, the dots around the cell also exhibit a small, but significant amount of luminescence but this does not prove that what can be seen are (aggregates of) the particles themselves. It is possible that they are debris from a cell that had taken some

nanoparticles. Overall it is likely that the particles interact with the cells because the distribution does not seem random, but the nature of this interaction is unknown. For example, whether or not they cross the cell membrane is still undetermined and more experiments will be required to answer that question.

4.4. Conclusion

An important objective was reached because the particles were rendered dispersible in phosphate buffer and observed in a biological context. First, the particles silica coated in presence of APTES were shown to possess NH_2 functionalities and particles silica coated in presence of a PEGsilane were stable in PBS. The cell culture of ovarian cancer cells went well and allowed the incubation of some cells in presence of the PEGylated nanoparticles which in turned allowed imaging to be performed. Although it seemed like the particles did interact with the cells the nature of the behaviour is unclear at the moment and requires a lot more experiments. However, this was an extremely important first step towards understanding and testing the full potential of theses nanoparticles as biolabels.

Chapter 5: Conclusion and future Work

In conclusion, a material was made that has great possibilities as a new upconverting biolabel operating within the biological window. It could open the door to new possibilities in the world of fluorescence microscopy.

As presented in Chapter 1, using wavelengths between 700 and 1000 nm (the biological window) offers some advantages in fluorescence microscopy, especially improving the possibilities to probe deeper into tissues. The principles behind multiphoton absorption and upconversion were also introduced with a special emphasis on upconversion within lanthanide ions systems because our nanoparticles take advantage of it.

The initial idea presented in Chapter 2 was to use a LaF_3:Yb,Tm nanoparticles because the combination of the Yb^{3+} and Tm^{3+} ions is well known to be suitable for upconversion where the excitation would be at 980 nm and the main emission at 800 nm. However, this emission was quenched when the citrate stabilized nanoparticles because of OH groups, from moisture or citrate ligands. The solution used by our groups for many years was to coat theses nanoparticles with hydrolysed silica and annealed them at high temperature to remove traces of water and OH groups. This method, as shown above, was successful in restoring the interesting optical properties to the Yb^{3+} and Tm^{3+} system but unfortunately the annealing step limited the surface modification of the particles preventing them from being water dispersible. This being an essential requirement for biolabels, it was decided to change the nanoparticle matrix.

This is presented in Chapter 3. Silica-coated $NaYF_4$:Yb,Tm nanoparticles were developed with the core in the hexagonal crystal phase because it has been known to enhance upconversion in lanthanide system and rendered the emission not as sensitive to quenching by OH groups. This meant the upconversion could be measured in suspension without the need of an annealing step which is very promising.

Finally, Chapter 4 presents two surface modifications performed on the silica coated $NaYF_4$:Yb,Tm nanoparticles. The first one was to incorporate NH_2 groups on the surface of the particles to be used as chemistry handles for further biofunctionalization while the second was to add PEG polymers to the surface to render the particles dispersible in phosphate buffer. Once both objectives were reached, cell culture of ovarian cancer cells were grown and incubated with the PEGylated version of the nanoparticles. These cells were then fixed on quartz slides and imaged using a modified fluorescence microscope to determine if the cells incorporated to nanoparticles. The preliminary results some kind of interactions between the nanoparticles and the cells but their nature is still under investigation.

In the future, our group projects to perform more incubation and imaging to optimize the conditions under which the particles could be incorporated by the cells. It is also planned to functionalize these nanoparticles with target specific antibody and study the specificity of the association of the particles with receptors on cancer cells.

Bibliography

1. Lindberg, A., Tungsten bulbs out in Ontario in 2012. *Ottawa Citizen* 2007.

2. Okelly, I., Seeing Ireland in a new light. *Irishtime* 2009.

3. Lakowicz, J. R., *Principles of Fluorescence Spectroscopy*. Third Edition ed.; Springer: Baltimore, MD, 2006; p 955.

4. Breeding, C. M.; Wang, W., Occurrence of the Si-V defect center in natural colorless gem diamonds. *Diamond and Related Materials* **2008,** 17, (7-10), 1335-1344.

5. Sivakumar, S.; van Veggel, F. C. J. M., Red, Green, and Blue Light Through Cooperative Up-Conversion in Sol-Gel Thin Films Made With $Yb_{0.80}La_{0.15}Tb_{0.05}F_3$ and $Yb_{0.80}La_{0.15}Eu_{0.05}F_3$ Nanoparticles. *Display Technology, Journal of* **2007,** 3, (2), 176-183.

6. Suyver, J. F.; Grimm, J.; van Veen, M. K.; Biner, D.; Kramer, K. W.; Gudel, H. U., Upconversion spectroscopy and properties of $NaYF_4$ doped with Er^{3+}, Tm^{3+} and/or Yb^{3+}. *Journal of Luminescence* **2006,** 117, (1), 1-12.

7. Konig, K., Multiphoton microscopy in life sciences. *Journal of Microscopy* **2000,** 200, (2), 83-104.

8. Sivakumar, S. Lanthanide-doped nanoparticles in sol-gel matrices; improved optical properties and new opportunities Ph.D., University of Victoria, Victoria, 2007.

9. Vetrone, F.; Boyer, J. C.; Capobianco, J. A.; Speghini, A.; Bettinelli, M., Effect of Yb^{3+} Codoping on the Upconversion Emission in Nanocrystalline $Y_2O_3:Er^{3+}$. *The Journal of Physical Chemistry B* **2003,** 107, (5), 1107-1112.

10. Sivakumar, S.; Diamente, P. R.; van Veggel, F. C. J. M., Silica-coated Ln(3+)-doped LaF_3 nanoparticles as robust down- and upconverting biolabels. *Chemistry-a European Journal* **2006,** 12, (22), 5878-5884.

11. Binnemans, K.; Van Deun, R.; Görller-Walrand, C.; Adam, J. L., Spectroscopic properties of trivalent lanthanide ions in fluorophosphate glasses. *Journal of Non-Crystalline Solids* **1998,** 238, (1-2), 11-29.

12. Stein, G.; Wurzberg, E., Energy-Gap Law in Solvent Isotope-Effect on Radiationless Transitions of Rare-Earth Ions. *Journal of Chemical Physics* **1975,** 62, (1), 208-213.

13. *CRC Handbook of Chemistry and Physics*. 77^{th} ed.; CRC press: Boca Raton, Florida, 1997.

14. Diamente, P. R. Development of water-soluble Ln^{3+}-doped LaF_3 nanoparticles as potential biolabels. M.Sc., University of Victoria, Victoria, 2008.

15. Ronda, C. R.; Jüstel, T.; Nikol, H., Rare earth phosphors: fundamentals and applications. *Journal of Alloys and Compounds* **1998,** 275-277, 669-676.

16. Boyer, J. C. Synthesis and Spectroscopy of Upconverting Lanthanide-Doped Nanocrystals. Ph.D., Concordia University, Montreal, 2006.

17. Qian, H.-S.; Zhang, Y., Synthesis of Hexagonal-Phase Core-Shell $NaYF_4$ Nanocrystals with Tunable Upconversion Fluorescence. *Langmuir* **2008,** 24, (21), 12123-12125.

18. Stouwdam, J. W. Lanthanide-doped nanoparticles as the active optical medium in polymer-based devices. Ph.D., University of Twente, Enschede, 2004.

19. Pichaandi, J., Private Comm. In 2008.

20. Microscope Time Line . http://nobelprize.org/educational_games/physics/microscopes/timeline/index.html (February 13th 2009),

21. Amiot, C. L.; Xu, S. P.; Liang, S.; Pan, L. Y.; Zhao, J. X. J., Near-infrared fluorescent materials for sensing of biological targets. *Sensors* **2008,** 8, (5), 3082-3105.

22. Denk, W.; Strickler, J. H.; Webb, W. W., Two-photon laser scanning fluorescence microscopy. *Science* **1990,** 248, (4951), 73-76.

23. Minsky, M., Memoir on Inventing the Confocal Scanning Microscope. *Scanning* **1988,** 10, 128-138.

24. Lazcka, O.; Campo, F. J. D.; Muñoz, F. X., Pathogen detection: A perspective of traditional methods and biosensors. *Biosensors and Bioelectronics* **2007,** 22, (7), 1205-1217.

25. Jamieson, T.; Bakhshi, R.; Petrova, D.; Pocock, R.; Imani, M.; Seifalian, A. M., Biological applications of quantum dots. *Biomaterials* **2007,** 28, (31), 4717-4732.

26. Smith, J. D.; Fisher, G. W.; Waggoner, A. S.; Campbell, P. G., The use of quantum dots for analysis of chick CAM vasculature. *Microvascular Research* **2007,** 73, (2), 75-83.

27. Y. Zheng, S. G. J. Y. Y., Synthesis and Cell-Imaging Applications of Glutathione-Capped CdTe Quantum Dots. *Advanced Materials* **2007,** 19, (3), 376-380.

28. Gerion, D.; Pinaud, F.; Williams, S. C.; Parak, W. J.; Zanchet, D.; Weiss, S.; Alivisatos, A. P., Synthesis and properties of biocompatible water-soluble silica-

coated CdSe/ZnS semiconductor quantum dots. *Journal of Physical Chemistry B* **2001,** 105, (37), 8861-8871.

29. Klostranec, J. M.; Chan, W. C. W., Quantum dots in biological and biomedical research: Recent progress and present challenges. *Advanced Materials* **2006,** 18, (15), 1953-1964.

30. Slowing, II; Trewyn, B. G.; Giri, S.; Lin, V. S. Y., Mesoporous silica nanoparticles for drug delivery and biosensing applications. *Advanced Functional Materials* **2007,** 17, (8), 1225-1236.

31. Zhu, L. Y.; Wu, W. W.; Zhu, M. Q.; Han, J. J.; Hurst, J. K.; Li, A. D. Q., Reversibly photoswitchable dual-color fluorescent nanoparticles as new tools for live-cell imaging. *Journal of the American Chemical Society* **2007,** 129, (12), 3524.

32. Kong, D. Y.; Wang, Z. L.; Lin, C. K.; Quan, Z. W.; Li, Y. Y.; Li, C. X.; Lin, J., Biofunctionalization of $CeF_3 : Tb^{3+}$ nanoparticles. *Nanotechnology* **2007,** 18, (7).

33. Chen, Y.; Chi, Y. M.; Wen, H. M.; Lu, Z. H., Sensitized luminescent terbium nanoparticles: Preparation and time-resolved fluorescence assay for DNA. *Analytical Chemistry* **2007,** 79, (3), 960-965.

34. Diamente, P. R.; van Veggel, F. C. J. M., Water-soluble Ln(3+)-doped LaF_3 nanoparticles: Retention of strong luminescence and potential as biolabels. *Journal of Fluorescence* **2005,** 15, (4), 543-551.

35. Chen, G. Y.; Zhang, Y. G.; Somesfalean, G.; Zhang, Z. G.; Sun, Q.; Wang, F. P., Two-color upconversion in rare-earth-ion-doped ZrO_2 nanocrystals. *Applied Physics Letters* **2006,** 89, (16).

36. Chatterjee, D. K.; Rufaihah, A. J.; Zhang, Y., Upconversion fluorescence imaging of cells and small animals using lanthanide doped nanocrystals. *Biomaterials* **2008,** 29, (7), 937-943.

37. Lim, S. F.; Riehn, R.; Ryu, W. S.; Khanarian, N.; Tung, C. K.; Tank, D.; Austin, R. H., In vivo and scanning electron microscopy imaging of upconverting nanophosphors in Caenorhabditis elegans. *Nano Letters* **2006,** 6, (2), 169-174.

38. Morgan, C. G.; Mitchell, A. C., Prospects for applications of lanthanide-based upconverting surfaces to bioassay and detection. *Biosensors & Bioelectronics* **2007,** 22, (8), 1769-1775.

39. Morgan, C. G.; Dad, S.; Mitchell, A. C., Present status of, and future prospects for, upconverting phosphors in proximity-based bioassay. *Journal of Alloys and Compounds* **2008,** 451, (1-2), 526-529.

40. Shan, J.; Chen, J.; Meng, J.; Collins, J.; Soboyejo, W.; Friedberg, J. S.; Ju, Y., Biofunctionalization, cytotoxicity, and cell uptake of lanthanide doped

hydrophobically ligated $NaYF_4$ upconversion nanophosphors. *Journal of Applied Physics* **2008,** 104, (9), 094308-7.

41. Chaplin, M. Water Absorption Spectrum. http://www.lsbu.ac.uk/water/vibrat.html (February 13th 2009),

42. Helmchen, F.; Denk, W., Deep tissue two-photon microscopy. *Nature Methods* **2005,** 2, (12), 932-940.

43. Motson, G. R.; Fleming, J. S.; Brooker, S., Potential applications for the use of lanthanide complexes as luminescent biolabels. In *Advances in Inorganic Chemistry: Including Bioinorganic Studies, Vol 55*, 2004; Vol. 55, pp 361-432.

44. Sammes, P. G.; Yahioglu, G., Modern bioassays using metal chelates as luminescent probes. *Natural Product Reports* **1996,** 13, (1), 1-28.

45. Biju, V.; Itoh, T.; Anas, A.; Sujith, A.; Ishikawa, M., Semiconductor quantum dots and metal nanoparticles: syntheses, optical properties, and biological applications. *Analytical and Bioanalytical Chemistry* **2008,** 391, (7), 2469-2495.

46. Kettering, M.; Winter, J.; Zeisberger, M.; Bremer-Streck, S.; Oehring, H.; Bergemann, C.; Alexiou, C.; Hergt, R.; Halbhuber, K. J.; Kaiser, W. A.; Hilger, I., Magnetic nanoparticles as bimodal tools in magnetically induced labelling and magnetic heating of tumour cells: an in vitro study. *Nanotechnology* **2007,** 18, (17).

47. Stouwdam, J. W.; Shan, J.; van Veggel, F. C. J. M.; Pattantyus-Abraham, A. G.; Young, J. F.; Raudsepp, M., Photostability of Colloidal PbSe and PbSe/PbS Core/Shell Nanocrystals in Solution and in the Solid State. *The Journal of Physical Chemistry C* **2007,** 111, (3), 1086-1092.

48. Dong, C. H.; Raudsepp, M.; van Veggel, F. C. J. M., Kinetically Determined Crystal Structures of Undoped and La^{3+}-Doped LnF_3. *Journal of Physical Chemistry C* **2009,** 113, (1), 472-478.

49. Sivakumar, S.; van Veggel, F.; Raudsepp, M., Sensitized emission from lanthanide-doped nanoparticles embedded in a semiconductor sol-gel thin film. *Chemphyschem* **2007,** 8, (11), 1677-1683.

50. Lo, A. Y. H.; Sudarsan, V.; Sivakumar, S.; van Veggel, F. C. J. M.; Schurko, R. W., Multinuclear solid-state NMR spectroscopy of doped lanthanum fluoride nanoparticles. *Journal of the American Chemical Society* **2007,** 129, (15), 4687-4700.

51. Dekker, R.; Klunder, D. J. W.; Borreman, A.; Diemeer, M. B. J.; Worhoff, K.; Driessen, A.; Stouwdam, J. W.; van Veggel, F. C. J. M., Stimulated emission and optical gain in LaF_3 : Nd nanoparticle-doped polymer-based waveguides. *Applied Physics Letters* **2004,** 85, (25), 6104-6106.

52. Kumar, G. A.; Chen, C. W.; Ballato, J.; Riman, R. E., Optical characterization of infrared emitting rare-earth-doped fluoride nanocrystals and their transparent nanocomposites. *Chemistry of Materials* **2007,** 19, (6), 1523-1528.

53. Yi, G. S.; Chow, G. M., Colloidal LaF_3 : Yb,Er, LaF_3 : Yb,Ho and LaF_3 : Yb,Tm nanocrystals with multicolor upconversion fluorescence. *Journal of Materials Chemistry* **2005,** 15, (41), 4460-4464.

54. Zhu, L.; Meng, I.; Cao, X. Q., Facile synthesis and photoluminescence of europium ion doped LaF_3 nanodisks. *European Journal of Inorganic Chemistry* **2007**, (24), 3863-3867.

55. Sudarsan, V.; Sivakumar, S.; van Veggel, F. C. J. M.; Raudsepp, M., General and convenient method for making highly luminescent sol-gel derived silica and alumina films by using LaF^3 nanoparticles doped with lanthanide ions (Er^{3+}, Nd^{3+}, and Ho^{3+}). *Chemistry of Materials* **2005,** 17, (18), 4736-4742.

56. Abdul Jalil, R.; Zhang, Y., Biocompatibility of silica coated $NaYF_4$ upconversion fluorescent nanocrystals. *Biomaterials* **2008,** 29, (30), 4122-4128.

57. Insin, N.; Tracy, J. B.; Lee, H.; Zimmer, J. P.; Westervelt, R. M.; Bawendi, M. G., Incorporation of Iron Oxide Nanoparticles and Quantum Dots into Silica Microspheres. *ACS Nano* **2008,** 2, (2), 197-202.

58. Koole, R.; van Schooneveld, M. M.; Hilhorst, J.; de Mello, D.; Celso; Hart, D. C.; van Blaaderen, A.; Vanmaekelbergh, D.; Meijerink, A., On the Incorporation Mechanism of Hydrophobic Quantum Dots in Silica Spheres by a Reverse Microemulsion Method. *Chem. Mater.* **2008,** 20, (7), 2503-2512.

59. Darbandi, M.; Lu, W. G.; Fang, J. Y.; Nann, T., Silica encapsulation of hydrophobically ligated PbSe nanocrystals. *Langmuir* **2006,** 22, (9), 4371-4375.

60. Bakalova, R.; Zhelev, Z.; Aoki, I.; Masamoto, K.; Mileva, M.; Obata, T.; Higuchi, M.; Gadjeva, V.; Kanno, I., Multimodal Silica-Shelled Quantum Dots: Direct Intracellular Delivery, Photosensitization, Toxic, and Microcirculation Effects. *Bioconjugate Chemistry* **2008,** 19, (6), 1135-1142.

61. Wei, Y.; Lu, F. Q.; Zhang, X. R.; Chen, D. P., Synthesis and characterization of efficient near-infrared upconversion Yb and Tm codoped $NaYF_4$ nanocrystal reporter. *Journal of Alloys and Compounds* **2007,** 427, (1-2), 333-340.

62. Lu, C. W.; Hung, Y.; Hsiao, J. K.; Yao, M.; Chung, T. H.; Lin, Y. S.; Wu, S. H.; Hsu, S. C.; Liu, H. M.; Mou, C. Y.; Yang, C. S.; Huang, D. M.; Chen, Y. C., Bifunctional Magnetic Silica Nanoparticles for Highly Efficient Human Stem Cell Labeling. *Nano Letters* **2007,** 7, (1), 149-154.

63. Zhuravlev, L. T., The surface chemistry of amorphous silica. Zhuravlev model. *Colloids and Surfaces A: Physicochemical and Engineering Aspects* **2000,** 173, (1-3), 1-38.

64. Ow, H.; Larson, D. R.; Srivastava, M.; Baird, B. A.; Webb, W. W.; Wiesner, U., Bright and Stable Core-Shell Fluorescent Silica Nanoparticles. *Nano Letters* **2005,** 5, (1), 113-117.

65. Yague, C.; Moros, M.; Grazu, V.; Arruebo, M.; Santamaria, J., Synthesis and stealthing study of bare and PEGylated silica micro- and nanoparticles as potential drug-delivery vectors. *Chemical Engineering Journal* **2008,** 137, (1), 45-53.

66. Zheng, L.; Xu, J.; Zhao, G.; Su, L.; Wu, F.; Liang, X., Bulk crystal growth and efficient diode-pumped laser performance of Yb3+:Sc2SiO5. *Applied Physics B: Lasers and Optics* **2008,** 91, (3), 443-445.

67. Sudarsan, V.; van Veggel, F. C. J. M.; Herring, R. A.; Raudsepp, M., Surface Eu^{3+} ions are different than "bulk" Eu^{3+} ions in crystalline doped LaF_3 nanoparticles. *Journal of Materials Chemistry* **2005,** 15, (13), 1332-1342.

68. Stober, W.; Fink, A.; Bohn, E., Controlled Growth of Monodisperse Silica Spheres in Micron Size Range. *Journal of Colloid and Interface Science* **1968,** 26, (1), 62-&.

69. *Jade*, 8.2; Materials Data inc: 2007.

70. Diamente, P. R.; Raudsepp, M.; van Veggel, F. C. J. M., Dispersible Tm^{3+}-doped nanoparticles that exhibit strong 1.47 μm photoluminescence. *Advanced Functional Materials* **2007,** 17, (3), 363-368.

71. Kramer, K. W.; Biner, D.; Frei, G.; Gudel, H. U.; Hehlen, M. P.; Luthi, S. R., Hexagonal Sodium Yttrium Fluoride Based Green and Blue Emitting Upconversion Phosphors. *Chemistry of Materials* **2004,** 16, (7), 1244-1251.

72. Nyk, M.; Kumar, R.; Ohulchanskyy, T. Y.; Bergey, E. J.; Prasad, P. N., High Contrast in Vitro and in Vivo Photoluminescence Bioimaging Using Near Infrared to Near Infrared Up-Conversion in Tm^{3+} and Yb^{3+} Doped Fluoride Nanophosphors. *Nano Letters* **2008,** 8, (11), 3834-3838.

73. Boyer, J.-C.; Vetrone, F.; Cuccia, L. A.; Capobianco, J. A., Synthesis of Colloidal Upconverting $NaYF_4$ Nanocrystals Doped with Er^{3+}, Yb^{3+} and Tm^{3+}, Yb^{3+} via Thermal Decomposition of Lanthanide Trifluoroacetate Precursors. *Journal of the American Chemical Society* **2006,** 128, (23), 7444-7445.

74. Kumar, R.; Nyk, M.; Ohulchanskyy, T. Y.; Flask, C. A.; Prasad, P. N., Combined Optical and MR Bioimaging Using Rare Earth Ion Doped $NaYF_4$ Nanocrystals. *Advanced Functional Materials* **2009,** 19, 853–859.

75. Yi, G. S.; Chow, G. M., Water-soluble $NaYF_4$: Yb,Er(Tm)/$NaYF_4$/polymer core/shell/shell nanoparticles with significant enhancement of upconversion fluorescence. *Chemistry of Materials* **2007,** 19, (3), 341-343.

76. Lin, W.; Fritz, K.; Guerin, G.; Bardajee, G. R.; Hinds, S.; Sukhovatkin, V.; Sargent, E. H.; Scholes, G. D.; Winnik, M. A., Highly Luminescent Lead Sulfide Nanocrystals in Organic Solvents and Water through Ligand Exchange with Poly(acrylic acid). *Langmuir* **2008,** 24, (15), 8215-8219.

77. Zhang, M.; Shi, S.; Meng, J.; Wang, X.; Fan, H.; Zhu, Y.; Wang, X.; Qian, Y., Preparation and Characterization of Near-Infrared Luminescent Bifunctional Core/Shell Nanocomposites. *Journal of Physical Chemistry C* **2008,** 112, (8), 2825-2830.

78. Qian, H.; Li, Z.; Zhang, Y., Multicolor polystyrene nanospheres tagged with up-conversion fluorescent nanocrystals. *Nanotechnology* **2008**, (25), 255601.

79. Han, Y.; Jiang, J.; Lee, S. S.; Ying, J. Y., Reverse Microemulsion-Mediated Synthesis of Silica-Coated Gold and Silver Nanoparticles. *Langmuir* **2008,** 24, (11), 5842-5848.

80. Jo, S.; Park, K., Surface modification using silanated poly(ethylene glycol)s. *Biomaterials* **2000,** 21, (6), 605-616.

81. Parak, W. J., Biological applications of colloidal nanoparticles. *Abstracts of Papers of the American Chemical Society* **2005,** 229, U656-U656.

82. Taylor, I.; Howard, A. G., Measurement of primary amine groups on surface-modified silica and their role in metal binding. *Analytica Chimica Acta* **1993,** 271, (1), 77-82.